POLITECNICO DI TORINO

Master's Degree in Mathematical Engineering



Master's Degree Thesis

Dynamics of disclination dipoles

Supervisors

Prof. Marco MORANDOTTI

Prof. Pierluigi CESANA

Candidate

Nicolò BRIATICO

Academic Year 2024-2025

Dopotutto la matematica non è altro che l'arte di dire che 0 = 0.

Abstract

In materials science, crystal lattice defects play a crucial role in determining the mechanical behavior of solids. These defects are generally classified into two main categories: dislocations and disclinations. Dislocations are related to translational defects, characterized by a Burgers vector, and are commonly divided into screw and edge types, depending on the orientation of the defect line with respect to the Burgers vector. On the other hand, disclinations are rotational defects associated with an angular mismatch, quantified by the Frank angle. In recent years disclinations have gained growing attention for their role in plasticity phenomena at small scales.

From a theoretical point of view, both dislocations and disclinations can be studied using variational methods. The minimizers of the isotropic elastic energies under the constraint of kinematic incompatibility can be modeled as a finite number of such defects. One key result is that the renormalized energy of a disclination dipole is equivalent to that of an edge dislocation under appropriate rescaling. Building on the variational framework of [10], we investigate the dynamics of a finite number of disclinations within a two-dimensional circular domain, assuming that the defects evolve according to the maximal dissipation criterion, in line with the Peierls-Nabarro approach [9, 11]. This implies that the dynamics follows a gradient flow structure, where the evolution is governed by the steepest descent of the renormalized energy.

Our main focus is the study of a dipole of disclinations with equal Frank angles in a unit disk. Due to symmetry, the problem can be reduced to two degrees of freedom: the position of the center of the dipole and the distance between the two defects. Through a detailed force analysis and a numerical implementation based on the explicit Euler scheme, we identify the stationary regimes and, correspondingly, classify the qualitative behavior of the system into three categories: a converging dipole with its center moving toward the origin; a converging dipole with its center approaching the boundary; and a diverging dipole where the defects move away from each other.

In the diverging regime, we compute an asymptotic estimate for the dipole separation, which exhibits a polynomial-in-time growth rate of the distance between the defects. In the converging regimes, on the contrary, we observe an exp(-exp) decay profile in the distance. Regardless of the converging regime, a particularly interesting outcome is that the collision of disclinations occurs only asymptotically in time. This behavior contrasts with that of dislocations, which are known to collide in finite time. Furthermore, in a specific case, we obtain an implicit formulation for the evolution of the dipole center. After a suitable transformation and a time renormalization, this formulation turns out to be mathematically equivalent to the dynamics of a screw dislocation in a circular domain [29], revealing a deep connection between the two types of defects.

In the final part of this thesis, we derive the dynamics of an edge dislocation from Eshelby's equivalence. In particular, to achieve this result, we extract the non-divergent contribution of the energy. By exploiting the maximal dissipation criterion, we obtain the dynamics of an edge dislocation in a circular domain. The obtained dynamics coincides with those derived from the time rescaling of the disclination dipole dynamics. From the analysis of the problem, it emerges that an edge dislocation, when located away from the center, tends to reach the boundary in finite time, while those positioned at the center of the domain remain there due to symmetry considerations.

Acknowledgements

First of all, I would like to thank Prof. Morandotti and Prof. Cesana for giving me the opportunity to work on this project, allowing me to discover the beauty in the smallest defects, as well as for their great support throughout this year. I would also like to thank Kyushu University and Politecnico di Torino for partially funding my two trips to Fukuoka: it was an incredibly formative experience that has contributed significantly to my personal growth and scientific development. In particular, most of the funding came from the JASSO scholarships offered within the Kyushu University Programm for Emerging Leaders in Science (Q-PELS). A special thanks goes to the Institute of Mathematics for Industry, an international joint usage and research facility located at Kyushu University, which gave me the opportunity to present part of the results discussed in this thesis at the 2024 Ajou-Kyushu-NIMS Joint workshop and the Forum "Math-for-Industry" 2025 - Challenge of Mathematics for Industry in the AI era, in South Korea.

Table of Contents

1	Intr	roduction	1
	1.1	Dislocations	3
	1.2	Disclinations	4
	1.3	Eshelby's equivalence	5
2	Var	iational model for crystalline defects	7
	2.1	Compatible elastic model	8
	2.2	Kinematic incompatibilities	9
	2.3		12
	2.4	From disclinations to dislocations	13
3	Dyr	namics of a dipole of disclinations	15
	3.1	Maximal dissipation criterion	15
	3.2	An isolated disclination	20
	3.3	Radial dipole	22
		3.3.1 Numerical simulations	28
		3.3.2 Region 1: boundary behaviour	33
		3.3.3 Region 2: convergent behavior	39
		3.3.4 Region 3: diverging behavior	43
	3.4		45
		3.4.1 Fixed distance behavior	46
		3.4.2 Fixed center of the dipole	47
4	Edg	ge dislocation	53
	4.1	The energy of an edge dislocation	54
	4.2	Dynamics of an edge dislocation	56
5	Con	aclusions and perspectives	61
Li	st of	Figures	63
Bi	bliog	graphy	65

Chapter 1

Introduction

In 1907, Vito Volterra published his seminal paper Sur l'équilibre des corps élastiques multiplement connexes [58], where he introduced a geometric and topological framework for describing defects in elastic bodies. His construction, later known as the Volterra's process, consists of cutting an infinite hollow cylinder along a surface, performing a rigid transformation (translation or rotation), and welding the cut surfaces back together. The resulting incompatibility models a defect: a dislocation if the transformation is translational (Figure 1.1a,b,c), or a disclination if it is rotational (Figure 1.1d,e,f).

Volterra's motivation was to explain the discrepancy between theoretical and experimental values of shear strength in crystalline solids. Classical elasticity, based on the assumption of perfect crystals, predicted critical stresses one to two orders of magnitude larger than those observed experimentally. The missing element was the presence of imperfections breaking lattice periodicity, which dramatically reduces the stress required for plastic deformation.

Although Volterra's approach was pioneering, the terminology dislocation was only introduced in 1927 by Love [37]. A decisive breakthrough occurred in 1934, when Taylor [56], Orowan [48], and Polányi [49] independently demonstrated that plastic deformation in metals is mediated by the collective motion of dislocations. Subsequently, Burgers introduced the concept of the Burgers vector [7], providing a precise quantitative characterization of dislocations and distinguishing between edge (Figure 1.1a,b) and screw types (Figure 1.1c).

The theory of rotational defects developed later: in the early 1950s, Frank and Read formulated a framework for characterizing rotational mismatches [20], introducing the *Frank angle* to quantify angular lattice distortions. This marked the birth of the modern theory of *disclinations*. In 1956, Hirsch, Horne, and Whelan [60] achieved the first experimental observation of dislocations through diffraction contrast microscopy (TEM), confirming the validity of Volterra's geometric description nearly fifty years after its proposal. The development of a systematic theory of

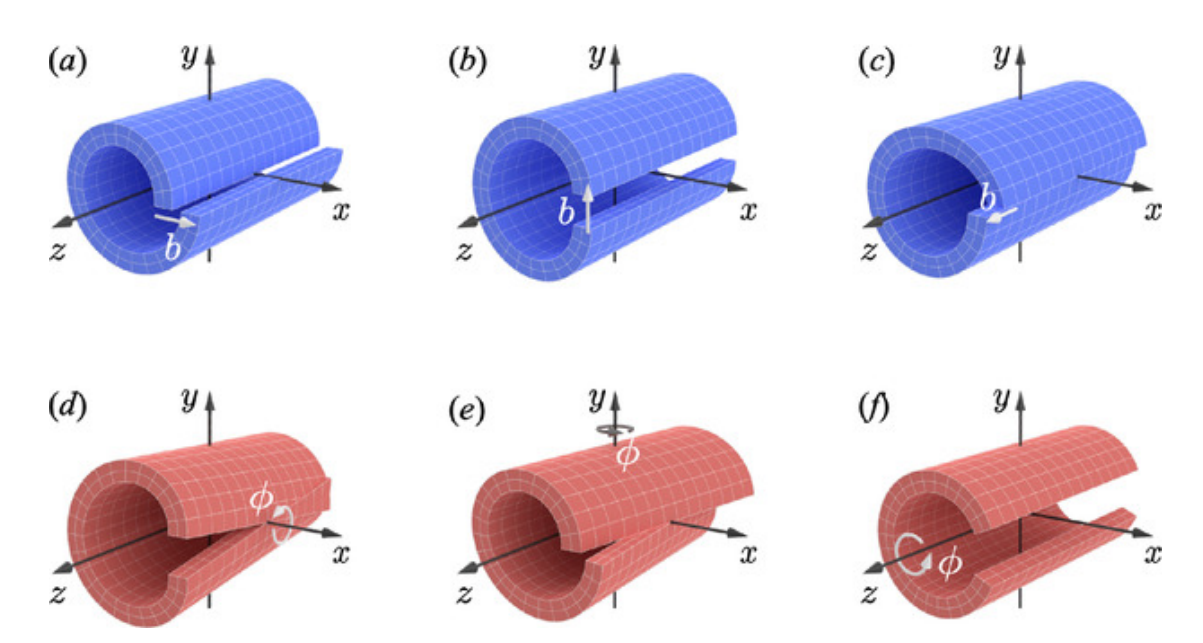


Figure 1.1: Schematic representation of the *Volterra's process*. A translational mismatch produces a *dislocation* (a,b,c), while a rotational mismatch produces a *disclination* (d,e,f). Where b is the *Burgers vector*, while here ϕ is the *Frank Angle*. Credit: [35, Figure 1].

disclinations was largely due to the work of de Wit [14, 15, 16, 17], who provided a rigorous mathematical formulation, later extended by Romanov [50]. These studies highlighted the fundamental role of disclinations in describing both plastic and microplastic phenomena in crystalline materials, explaining the growing attention that disclinations currently receive in materials science and applied mathematics.

Defects are ubiquitous in nature, from the microstructure of metals to macroscopic objects, such as footballs or maize cobs, and play a crucial role in determining the mechanical properties of materials. In particular, interactions between defects can lead to emergent material behaviors, such as strain hardening and local brittleness. A paradigmatic example is the annihilation of a pair of dislocations, which locally inhibits plastic slip. This type of interaction underlies the celebrated *Eshelby equivalence* [19], which relates an edge dislocation to a dipole of disclinations. A formal mathematical proof has been presented in [10], and it has renewed interest in the interplay between these two classes of defects.

In this chapter, we present the most significant and well-known properties of dislocations and disclinations, highlighting both the results established in the existing literature and those derived in the present thesis. Furthermore, we introduce the key aspects and distinctive features of Eshelby's equivalence.

1.1 Dislocations

We now return to Volterra's construction and focus on Figure 1.1a,b,c, which correspond to a *translational* defect. Consider a hollow cylindrical body cut along a generator; depending on how the cut surfaces are re-glued together, one obtains either an *edge* (cases a, b) or a *screw* dislocation (case c).

A screw dislocation is so named because of the helical distortion of the lattice around the dislocation line, resembling a screw. In contrast, an edge dislocation is created by the insertion or removal of a half-plane of atoms, producing a wedge-like lattice distortion. Dislocations are graphically represented by a line indicating the defect and a $Burgers\ vector\ b$, a quantity introduced by Burgers [7] to characterize the magnitude and direction of lattice distortion. Mathematically, the Burgers vector is defined as the closure failure of a circuit surrounding the defect:

$$b = \oint_{\Gamma} \nabla u(x) \, \mathrm{d}x,$$

where Γ is a closed contour encircling the dislocation line, and u is the displacement field. Edge dislocations are characterized by a Burgers vector *perpendicular* to the defect line, while screw dislocations have a Burgers vector *parallel* to the defect line.

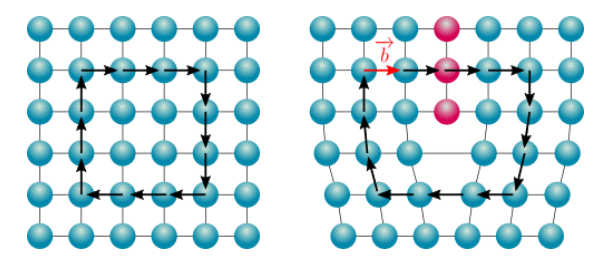


Figure 1.2: On the left a perfect crystal, where the black arrows represent the circuit Γ ; on the right a crystal with an edge dislocation, where the red path represents the line defect, and b is the Burgers vector. Credit: [23, Figure 9].

From an energetic standpoint, dislocations are costly defects: their elastic energy diverges logarithmically with the core-radius. This singular behavior makes it necessary to introduce a variational technique known as the *core-radius approach* (for further details, see [8]).

In the case of screw dislocations, it is known that a single dislocation within a domain tends to be expelled in finite time, while a dipole of dislocations tends to collide in finite time. Regarding edge dislocations, in this thesis we will show that the behavior of a single edge dislocation is analogous: it tends to be expelled from the domain in finite time.

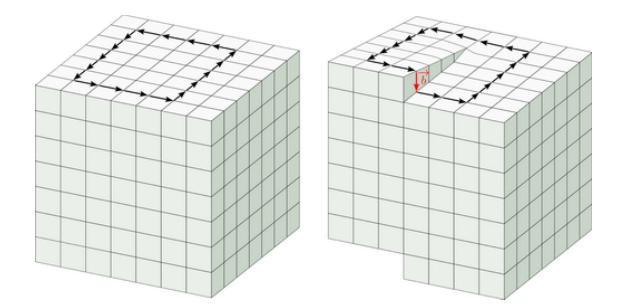


Figure 1.3: On the left a perfect crystal, where the black arrows represent the circuit Γ ; on the right a crystal with screw dislocation where b is the Burgers vector. Credit: [23, Figure 12].

1.2 Disclinations

We now turn to Figure 1.1.d,e,f, corresponding to rotational defects. Consider an infinite hollow cylinder; if a triangular wedge of material is inserted and the cut surfaces are reattached while constraining the lattice to remain flat, atoms must shift to accommodate the extra wedge, resulting in a negative planar wedge disclination. Conversely, removing a wedge of material produces a positive planar wedge disclination [50].

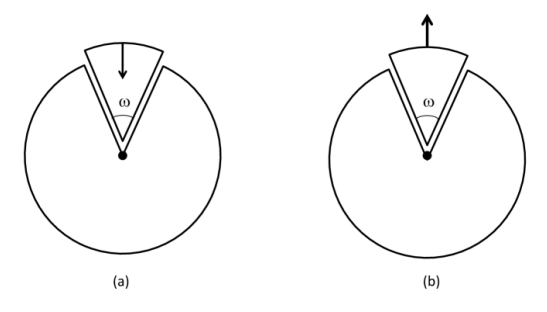


Figure 1.4: Formation of a planar wedge disclination: (a) is the negative disclination, while (b) is the positive one. Credit: [61, Figure 3].

Isolated disclinations are extremely energetic: their elastic energy diverges linearly with the area of the sample [54, Formula (2.22)]. making them rare in crystalline solids. On the other hand, the scenario with a pair of disclinations with opposite Frank angle, known as dipole, is more common. In [11] the behavior of a single disclination and a symmetric disclination dipole in a unit disk is analyzed. Furthermore, in this thesis, we analyze the behavior of a radial disclination dipole and its dynamical relationship with an edge dislocation. In particular, it has been

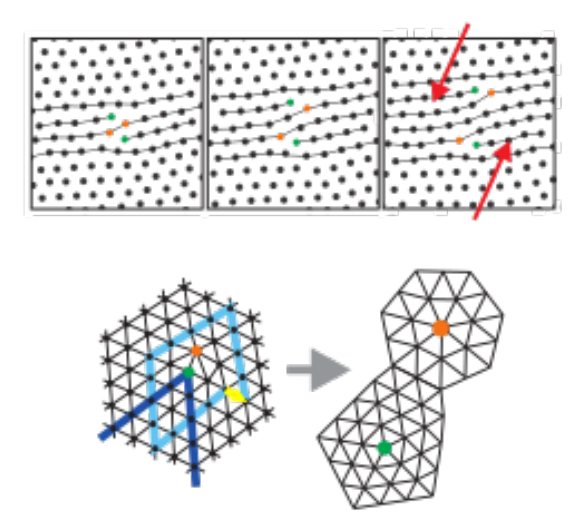


Figure 1.5: Scheme of a sample with disclinations. The green point represent a positive disclination, while the orange one a negative disclination. Credit: [32].

shown that single disclinations tend to be expelled from the domain in infinite time, whereas a dipole of disclinations may collapse in infinite time.

First experimental evidence for disclinations only became available in 1974 in nematic liquid crystals [38, 57, 62]. Nevertheless, they arise naturally in many physical systems, also including grain boundaries in polycrystals [3, 51], biological structures [24, 44], and engineered tessellations (e.g. Biodôme de Montréal), where they induce geometric effects, such as curvature.

1.3 Eshelby's equivalence

Over the years, several relationships between different types of defects have been studied (see [14, 26, 27, 31, 43, 50] for historical and technical overviews). Of particular interest in this work is the equivalence proposed by Eshelby in [19], which states that a dipole of disclinations behaves, in the limit where the distance between the two singularities tends to zero, as an edge dislocation. This equivalence suggests a deep geometric and energetic equivalence between dislocations and disclinations, despite their fundamentally different characterizations.

This relationship is particularly important for two main reasons: first, it allows us to elegantly derive the formulation for the dynamics of an edge dislocation, which was previously unknown; second, it enables a more detailed investigation of plasticity and microplasticity phenomena associated with the presence of such defects. In particular, the link with plasticity is discussed in [2, 21, 34, 42, 50, 55],

where it is observed that, as the number of defects in the domain increases, a plastic behavior emerges. Based on this equivalence, it would therefore be possible to gain additional insight by understanding how the presence of such defects influences plastic behavior. Clearly, a deeper understanding of this phenomenon would have significant applications in engineering and materials science, providing further knowledge for the design of innovative materials, such as graphene [51].

This energetical equivalence bridges two fundamental types of lattice defects, linking disclinations, rare but powerful sources of rotational distortion, to dislocations. In Chapter 2, we analyze the mathematical model and some sketches of the proof strategy from [10, Section 4] that establish this equivalence rigorously.

Chapter 2

Variational model for crystalline defects

The study of crystalline defects has developed along fragmented paths, driven both by the evolution of experimental techniques and by advances in continuum modeling. Discrete and continuum descriptions have been proposed for both dislocations and disclinations (see, e.g., [54] for dislocations and [50] for disclinations). However, classical linearized continuum models, while mathematically tractable, often suffer from either excessive complexity or insufficient mechanical fidelity at the defect scale, reducing their effectiveness in delivering quantitative, predictive insight.

A turning point came with the introduction of Γ -convergence (see [12, 13]), which provided a powerful variational framework to pass from discrete to continuum and to extract effective models in singularly perturbed problems. Within this framework, Cermelli and Leoni [8] addressed the issue of the *infinite elastic energy* associated with line defects by introducing what is now known as the *core-radius regularization approach*: the energy is analyzed by removing a disk, or core, of radius $\varepsilon > 0$ around each singularity, and the contributions to the energy that diverge in the limit as $\varepsilon \to 0$ are isolated to define a finite, renormalized energy/force. This paradigm paved the way for a series of works on linear models for screw dislocations [21, 40] and nonlinear variants [41], and it underpins dissipative evolutions driven by renormalized forces under the maximal dissipation criterion [9].

In this chapter we adopt the viewpoint proposed in [9], which is both concise and robust: it makes the role of incompatibilities transparent, yields the governing PDE as Euler–Lagrange conditions, and is well suited for singular limits. We first set up the compatible elastic model, then introduce kinematic incompatibilities that encode point defects, and finally derive the PDE formulation. We then use this framework to explain, in a precise asymptotic sense, how disclination dipoles converge to edge dislocations, following the analysis in [10].

2.1 Compatible elastic model

Let $\Omega \subset \mathbb{R}^2$ be a bounded, simply connected domain with $\partial \Omega \in \mathcal{C}^2$. We work in planar linearized elasticity (plane strain kinematics), placing the reference frame on the cross-section of the body so that line defects appear as points in $\Omega \subset \mathbb{R}^2$. The displacement is $u \in H^1(\Omega; \mathbb{R}^2)$, with linearized strain

$$\epsilon := \nabla^{\text{sym}} u = \frac{1}{2} (\nabla u + \nabla u^{\top}) \in L^2(\Omega; \mathbb{R}^{2 \times 2}_{\text{sym}}).$$
(2.1)

For an isotropic material with Lamé constants λ and μ , the Cauchy stress is

$$\sigma = \mathbb{C}\epsilon = \lambda \operatorname{tr}(\epsilon) I + 2\mu \epsilon, \tag{2.2}$$

with

$$\mu = \frac{E}{2(1+\nu)}$$
 and $\lambda = \frac{E\nu}{(1+\nu)(1-2\nu)}$,

where E > 0 is the Young's modulus and $\nu \in (-1, \frac{1}{2})$ is the Poisson ratio. An equivalent formulation of (2.2) is

$$\sigma = \frac{E\nu}{(1-\nu)(1-2\nu)}\operatorname{cof}\epsilon + \frac{E}{1-2\nu}\epsilon,$$

and its inverse formulation reads

$$\epsilon = \mathbb{C}^{-1}\sigma = \frac{1 - \nu^2}{E}\sigma - \frac{(1 + \nu)\nu}{E}\operatorname{cof}\sigma, \tag{2.3}$$

where we define $cof : \mathbb{R}^{2x2} \mapsto \mathbb{R}^{2x2}$ so that

$$\begin{pmatrix} m_{11} & m_{12} \\ m_{21} & m_{22} \end{pmatrix} = m \mapsto \operatorname{cof} m = \begin{pmatrix} m_{22} & -m_{21} \\ -m_{12} & m_{11} \end{pmatrix}.$$

The elastic energy reads

$$\mathcal{E}(u;\Omega) = \frac{1}{2} \int_{\Omega} \sigma : \epsilon \, dx = \frac{1}{2} \int_{\Omega} \left(\lambda \operatorname{tr}(\epsilon)^2 + 2\mu \, |\epsilon|^2 \right) dx. \tag{2.4}$$

We now introduce the Airy potential $v \in H^2(\Omega)$ so that

$$\sigma_{11} = \partial_y^2 v, \qquad \sigma_{22} = \partial_x^2 v, \qquad \sigma_{12} = \sigma_{21} = -\partial_{xy}^2 v.$$
 (2.5)

By using the Airy potential it is possible to express σ in terms of v

$$\sigma = \sigma[v] = A(v), \tag{2.6}$$

where A is defined as

$$A(v) = \operatorname{cof}(\nabla^2 v) = \begin{pmatrix} \partial_{yy}^2 v & -\partial_{xy}^2 v \\ -\partial_{yx}^2 v & \partial_{xx}^2 v \end{pmatrix}. \tag{2.7}$$

From (2.7) we can observe that the condition

$$\operatorname{div} \sigma[v] = \operatorname{div} \left(\operatorname{cof} \left(\nabla^2 v\right)\right) = 0 \text{ in } \Omega \tag{2.8}$$

is always satisfied. In terms of v, the energy in (2.4) can be written as

$$\mathcal{G}(v;\Omega) = \frac{1}{2} \frac{1+\nu}{E} \int_{\Omega} \left(|\nabla^2 v|^2 - \nu (\Delta v)^2 \right) dx, \tag{2.9}$$

which is strictly convex, bounded below and coercive [10, Section 2]. The traction-free boundary condition

$$\sigma n = 0$$
 on $\partial \Omega$

translates, using (2.6), into

$$0 = \sigma[v] n = \operatorname{cof}(\nabla^2 v) n = \begin{pmatrix} \partial_{yy}^2 v & -\partial_{xy}^2 v \\ -\partial_{yx}^2 v & \partial_{xx}^2 v \end{pmatrix} \begin{pmatrix} n_1 \\ n_2 \end{pmatrix} = \nabla^2 v t \qquad (2.10)$$

where n is the outward unit normal and t:=Rn is the unit tangent obtained via the $\pi/2$ -rotation $R=\left(\begin{smallmatrix}0&-1\\1&0\end{smallmatrix}\right)$.

2.2 Kinematic incompatibilities

Let us consider a field $V = (V_1, V_2) : \Omega \mapsto \mathbb{R}^2$, we define

$$\operatorname{curl} V \coloneqq \partial_x V_2 - \partial_y V_1.$$

If M is a 2×2 matrix, we introduce the operator

$$\operatorname{Curl} M = (\operatorname{curl} M^{(1)}, \operatorname{curl} M^{(2)}),$$

where $M^{(r)}$ is the r-th row of M. Let $u \in \mathcal{C}^3$, we set

$$\beta := \nabla u$$

and decompose it in

$$\beta = \epsilon + \omega, \tag{2.11}$$

with ϵ defined in (2.1) and $\omega := \frac{1}{2}(\beta - \beta^{\top})$. By construction,

$$\omega = \begin{pmatrix} 0 & f \\ -f & 0 \end{pmatrix}, \tag{2.12}$$

for some $f \in \mathcal{C}^2$ and it follows that $\operatorname{Curl} \omega = \nabla f$. By applying Curl to (2.11), and recalling that $\operatorname{Curl} \nabla = 0$, it follows that

$$\operatorname{Curl} \epsilon = -\nabla f. \tag{2.13}$$

By applying the curl to (2.13), one has the de Saint-Venant condition [53]:

$$\operatorname{curl}\operatorname{Curl}\epsilon = 0. \tag{2.14}$$

Vice versa, it is possible to prove that from (2.14), with $\epsilon \in C^2(\Omega, \mathbb{R}^{2x^2}_{\text{sym}})$, it follows that $u \in C^3(\Omega, \mathbb{R}^2)$ such that $\epsilon = \nabla^{\text{sym}} u$. In particular, in [10, Proposition 1.1] it is shown that it is possible to extend (2.14) also to $u \in H^1(\Omega, \mathbb{R}^2)$, the natural Sobolev space for applying the direct method of calculus of variations. We consider $H^1(\Omega, \mathbb{R}^2)$ to be the natural functional setting for the application of the direct method in the calculus of variations, due to several key properties:

- (i) $H^1(\Omega, \mathbb{R}^2)$ is a reflexive Banach space, which ensures the weak compactness of bounded sequences, a fundamental requirement for extracting convergent subsequences of minimizing sequences;
- (ii) many energy functionals arising in elasticity and mechanics are coercive and lower semicontinuous with respect to the weak topology of H^1 , ensuring the existence of minimizers via the direct method;
- (iii) in problems where the strain tensor $\epsilon = \nabla^{\text{sym}} u$ appears, the weak differentiability of $u \in H^1(\Omega, \mathbb{R}^2)$ is sufficient to give meaning to $\epsilon \in L^2(\Omega, \mathbb{R}^{2\times 2}_{\text{sym}})$, so that the energy functional depending on ϵ is well-defined.

Hence, $H^1(\Omega, \mathbb{R}^2)$ provides the minimal regularity assumptions under which the variational problem is well-posed and the standard tools of functional analysis can be effectively applied.

Let us now suppose that $f \in L^2(\Omega)$ and consider the operator ∇ in the sense of distribution. By denoting with $\mathcal{D}'(\Omega)$ the distributions, we can state that

Curl
$$\beta = \alpha$$
 with $\alpha \in \mathcal{D}'(\Omega)$,

so it follows that

$$\operatorname{Curl} \epsilon = \alpha - \nabla f.$$

In the same fashion, we suppose that

$$\operatorname{Curl} \nabla f = \theta$$
, with $\theta \in \mathcal{D}'(\Omega)$,

then it follows that the de Saint-Venant condition now reads

$$\operatorname{curl}\operatorname{Curl}\epsilon = \operatorname{curl}\alpha - \theta. \tag{2.15}$$

For finitely many point defects $J, K \in \mathbb{N}$ we take

$$\alpha := \sum_{j=1}^{J} b_j \, \delta_{x^j}, \qquad \theta := \sum_{k=1}^{K} s_k \, \delta_{y^k}, \qquad (2.16)$$

where α is the dislocation measure and θ is the disclination measure. Here $b_j \in \mathbb{R}^2$ is a Burgers vector, $s_k \in \mathbb{R}$ is a Frank angle, and δ_z is the Dirac delta centered at z the position of the defect. In this chapter we focus only on disclinations, so we set $\alpha \equiv 0$ in (2.15). The differential problem describing the disclination incompatibility reads

$$\begin{cases} \operatorname{curl} \operatorname{Curl} \epsilon = -\theta & \text{in } \Omega, \\ \operatorname{div} \sigma = 0 & \text{in } \Omega, \\ \sigma n = 0 & \text{on } \partial \Omega. \end{cases}$$
 (2.17)

From (2.3) and (2.6) it follows that

$$\epsilon = \frac{1+\nu}{E} \begin{pmatrix} (1-\nu)\sigma_{11} - \nu\sigma_{22} & \sigma_{12} \\ \sigma_{12} & (1-\nu)\sigma_{22} - \nu\sigma_{11} \end{pmatrix}$$
$$= \frac{1+\nu}{E} \begin{pmatrix} (1-\nu)\partial_{yy}^{2}v - \nu\partial_{xx}^{2}v & -\partial_{xy}^{2}v \\ -\partial_{xy}^{2}v & (1-\nu)\partial_{xx}^{2}v - \nu\partial_{yy}^{2}v \end{pmatrix}$$

By applying the de Saint-Venant condition, we obtain that

$$\operatorname{Curl} \epsilon = \begin{pmatrix} \operatorname{curl} \epsilon^{(1)} \\ \operatorname{curl} \epsilon^{(2)} \end{pmatrix} = \begin{pmatrix} \partial_x \epsilon_{12} - \partial_y \epsilon_{11} \\ \partial_x \epsilon_{22} - \partial_y \epsilon_{12} \end{pmatrix}$$

$$\operatorname{curl} \operatorname{Curl} \epsilon = \partial_x (\partial_x \epsilon_{22} - \partial_y \epsilon_{12}) - \partial_y (\partial_x \epsilon_{12} - \partial_y \epsilon_{11})$$
$$= \partial_{xx}^2 \epsilon_{22} - 2 \partial_{xy}^2 \epsilon_{12} + \partial_{yy}^2 \epsilon_{11}$$

$$\begin{aligned} \operatorname{curl} \operatorname{Curl} \epsilon[v] &= \frac{1+\nu}{E} \partial_{xx}^2 \left[(1-\nu) \partial_{xx}^2 v - \nu \partial_{yy}^2 v \right] \\ &+ 2 \frac{1+\nu}{E} \partial_{xy}^2 \partial_{xy}^2 v + \frac{1+\nu}{E} \partial_{yy}^2 \left[(1-\nu) \partial_{yy}^2 v - \nu \partial_{xx}^2 v \right] \\ &= \frac{1+\nu}{E} \left[(1-\nu) (\partial_{xxxx}^4 v + \partial_{yyyy}^4 v + 2 \partial_{xxyy}^4 v) \right] \\ &= \frac{1-\nu^2}{E} (\partial_{xxxx}^4 v + \partial_{yyyy}^4 v + 2 \partial_{xxyy}^4 v) \\ &= \frac{1-\nu^2}{E} \Delta^2 v. \end{aligned}$$

So now the problem reads

$$\frac{1-\nu^2}{E}\Delta^2 v = -\theta \quad \text{in } \Omega. \tag{2.18}$$

Combining (2.8), (2.10), and (2.18), we can express (2.17) as

$$\begin{cases} \frac{1-\nu^2}{E} \Delta^2 v = -\theta & \text{in } \Omega, \\ \nabla^2 v \, t = 0 & \text{on } \partial \Omega. \end{cases}$$
 (2.19)

2.3 Variational formulation with incompatibilities

The variational functional that encodes the elastic response and the incompatibility source is

$$\mathcal{I}^{\theta}(v;\Omega) := \mathcal{G}(v;\Omega) + \langle \theta, v \rangle$$

$$:= \frac{1}{2} \frac{1+\nu}{E} \int_{\Omega} \left(|\nabla^{2} v|^{2} - \nu (\Delta v)^{2} \right) dx + \sum_{k=1}^{K} s_{k} v(y^{k}), \qquad (2.20)$$

to be minimized over $v \in H^2(\Omega)$ subject to the traction-free boundary condition (2.10). In particular, \mathcal{G} is the elastic contribute in (2.20), whereas the linear term $\langle \theta, v \rangle$ is the natural duality pairing between the disclination measure and the Airy potential.

A standard computation shows that for any $\varphi \in H_0^2(\Omega)$ with $(\nabla^2 \varphi) t = 0$ on $\partial \Omega$,

$$\frac{\mathrm{d}}{\mathrm{d}\eta}\Big|_{\eta=0} \mathcal{I}^{\theta}(v+\eta\varphi) = \frac{\mathrm{d}}{\mathrm{d}\eta}\Big|_{\eta=0} \left(\mathcal{G}(v+\eta\varphi;\Omega) + \langle \theta, v+\eta\varphi \rangle \right)
= \frac{\mathrm{d}}{\mathrm{d}\eta}\Big|_{\eta=0} \left(\frac{1}{2} \frac{1+\nu}{E} \int_{\Omega} \left[(\nabla^{2}v + \eta\nabla^{2}\varphi)^{2} - \nu(\Delta v + \eta\Delta\varphi)^{2} \right] \mathrm{d}x
+ \langle \theta, v \rangle + \eta \langle \theta, \varphi \rangle \right)
= \frac{1+\nu}{E} \int_{\Omega} \left(\nabla^{2}v \nabla^{2}\varphi - \nu\Delta v\Delta\varphi \right) \mathrm{d}x + \langle \theta, \varphi \rangle
= \frac{1-\nu^{2}}{E} \int_{\Omega} \Delta v \Delta\varphi \, \mathrm{d}x + \langle \theta, \varphi \rangle.$$

Integrating by parts twice and using the traction-free boundary condition yields the Euler–Lagrange equation

$$\frac{1-\nu^2}{E}\Delta^2 v = -\theta \text{ in } \Omega, \qquad \nabla^2 v \, t = 0 \text{ on } \partial\Omega.$$
 (2.21)

Equation (2.21) is precisely the distributional form of the incompatibility relation $\operatorname{curl} \operatorname{Curl} \epsilon = -\theta$, expressed through the Airy function (2.5).

2.4 From disclinations to dislocations

We now show how an edge dislocation emerges as the limit of a disclination dipole. Fix a point $x \in \Omega$ and a unit vector $e \in \mathbb{S}^1$; for h > 0 small, we define the dipole measure

$$\theta^h = s \left(\delta_{x + \frac{h}{2}e} - \delta_{x - \frac{h}{2}e} \right),$$

with Frank angle $s \in \mathbb{R}$. The associated energy is

$$\mathcal{I}^{\theta^h}(v;\Omega) = \frac{1}{2} \frac{1+\nu}{E} \int_{\Omega} \left(|\nabla^2 v|^2 - \nu (\Delta v)^2 \right) dx + s \left[v \left(x + \frac{h}{2} e \right) - v \left(x - \frac{h}{2} e \right) \right].$$

To analyze the relevant rescaling for the Airy stress function, we assume $v \mapsto hw$. It follows that

$$\mathcal{G}(hw;\Omega) = \frac{1}{2} \frac{1+\nu}{E} \int_{\Omega} \left(|\nabla^{2}(hw)|^{2} - \nu(\Delta(hw))^{2} \right) dx$$

$$= \frac{1}{2} \frac{1+\nu}{E} h^{2} \int_{\Omega} \left(|\nabla^{2}w|^{2} - \nu(\Delta w)^{2} \right) dx$$

$$= h^{2} \mathcal{G}(w;\Omega)$$
(2.22)

and

$$\langle \theta^h, hw \rangle = h \langle \theta^h, w \rangle. \tag{2.23}$$

Motivated by the emerging h^2 term in (2.22), we introduce the following rescaled functional:

$$\mathcal{J}^{h}(w;\Omega) := \frac{1}{h^{2}} \mathcal{I}^{\theta^{h}}(hw;\Omega) = \mathcal{G}(w;\Omega) + \left\langle \frac{\theta^{h}}{h}, w \right\rangle = \mathcal{I}^{\theta_{h}/h}(w;\Omega)$$

$$= \frac{1}{2} \frac{1+\nu}{E} \int_{\Omega} \left(|\nabla^{2}w|^{2} - \nu(\Delta w)^{2} \right) dx + s \frac{w\left(x + \frac{h}{2}e\right) - w\left(x - \frac{h}{2}e\right)}{h}.$$
(2.24)

As $h \to 0$, the last term converges to the directional derivative of w:

$$\frac{w\left(x+\frac{h}{2}e\right)-w\left(x-\frac{h}{2}e\right)}{h} \longrightarrow \partial_e w(x), \tag{2.25}$$

which can be expressed, in the sense of distributions, using the derivative of a Dirac delta, as

$$\partial_e w(x) = -\langle \partial_e \delta_x, w \rangle.$$

Therefore, \mathcal{J}^h converges to the limiting functional

$$\mathcal{I}_{\text{edge}}(w;\Omega) = \frac{1}{2} \frac{1+\nu}{E} \int_{\Omega} \left(|\nabla^2 w|^2 - \nu (\Delta w)^2 \right) dx - s \langle \partial_e \delta_x, w \rangle. \tag{2.26}$$

Regarding the boundary condition $\nabla^2 v t = 0$, we observe that, due to the parameterization of v and the linearity of the operator ∇ , it follows that

$$0 = \nabla^2 v \, t = \nabla^2 (hw) \, t = h \, \nabla^2 w \, t.$$

The Euler–Lagrange equation associated with (2.26) is

$$\frac{1-\nu^2}{E}\Delta^2 w = s\,\partial_e \delta_x \text{ in } \Omega, \qquad \nabla^2 w\,t = 0 \text{ on } \partial\Omega, \tag{2.27}$$

which is the Airy formulation for an edge dislocation located at x. Geometrically, the Burgers vector b is orthogonal to the dipole axis e (up to the $\pi/2$ rotation relating σ and $\nabla^2 v$), with magnitude proportional to |s|:

$$b = sRe, (2.28)$$

consistent with the fact that an edge dislocation arises as the limit of two opposite disclinations approaching along e.

Remark 2.4.1 (Eshelby's equivalence). *Identity* (2.27) shows that the energy of a disclination dipole rescaled by h^2 and its corresponding governing PDE converge to those of an edge dislocation as the distance $h \to 0$, thus establishing Eshelby's equivalence in a rigorous variational sense (see [10, Section 4] for a complete proof, recovery sequences, and compactness).

Chapter 3

Dynamics of a dipole of disclinations

3.1 Maximal dissipation criterion

Defects in crystalline lattices, such as dislocations, disclinations, vacancies, and grain boundaries, are known to significantly alter the mechanical, electrical, and thermal properties of materials. These defects can, for instance, act as stress concentrators [36, 59], or reduce the thermal [28, 52] and electrical [18] conductivity. In particular, with regard to disclinations, in [2, 34, 42, 50] is observed that plastic phenomena in crystalline solids can be attributed to defects and, in particular, to the breaking of rotational symmetry. Understanding the dynamics of these defects, namely, how they move, interact with each other, or with the domain boundaries, is therefore essential for a deeper investigation of the mechanisms governing plasticity in crystalline materials [55].

The evolution of defect dynamics can be described through the so-called maximal dissipation criterion (as done, e.g., in [9, 11, 29]), a variational principle that provides a theoretical framework consistent with the second law of thermodynamics. This principle allows one to derive motion laws for defects or plastic deformations that are energetically admissible within the system [39]. It is applicable both in discrete models and in continuum formulations, and has been successfully employed, for instance, in the study of screw dislocations within the Peierls–Nabarro framework, where the evolution is governed by the so-called Peach–Koehler force [4, 5, 6, 30, 46].

In this thesis, we aim to extend the application of the maximal dissipation criterion to the case of disclinations, as recently proposed in [11]. According to this approach, given the minimal energy associated with the system as a function of the defect position, the dynamics is obtained by imposing that the velocity of the defect is

proportional to the negative gradient of the energy with respect to its position, thereby ensuring a monotonic dissipation of energy over time.

Let

$$\bar{v} = \arg\min\left\{\mathcal{I}^{\theta}(v;\Omega) \,\middle|\, v \in H_0^2(\Omega)\right\}$$

be the configuration that minimizes the elastic energy under homogeneous boundary conditions $(v = \partial_n v = 0 \text{ on } \partial\Omega)$. In particular, we consider $v \in H_0^2(\Omega)$, as this is the minimum regularity required to guarantee that the energy is in L^2 . Moreover, as demonstrated in [10, Proposition A.2], we have the following equivalence:

$$\nabla^2 v \, t = 0 \quad \text{on } \partial\Omega \iff v = a, \quad \partial_n v = \partial_n a \quad \text{on } \partial\Omega, \tag{3.1}$$

for some affine function a. By exploiting the fact that the problem is closed under rigid body motions, we can choose a = 0 and thus minimize over $H_0^2(\Omega)$. Since \bar{v} is also a solution to the associated differential problem in (2.21), we can apply Clapeyron's theorem, which implies that

$$\mathcal{G}(\bar{v};\Omega) = -\frac{1}{2} \langle \theta, \bar{v} \rangle. \tag{3.2}$$

Clapeyron's theorem, in this context, establishes a fundamental relationship between the elastic energy stored in the system and the work done by the sources of incompatibility on the deformation \bar{v} . More precisely, the term $\langle \theta, \bar{v} \rangle$ can be interpreted as the mechanical work exerted by the disclinations (represented by θ) on the resulting elastic configuration. This principle is consistent with the classical energetic interpretation in linear elasticity theory and is essential for deriving explicit formulas for the energy in the presence of localized defects.

In the special case where the domain Ω is the disk of radius R > 0 centered at the origin, $\Omega = B_R(0)$, the solution \bar{v} corresponds to the one obtained in the so-called *clamped disk problem*, as described in [45]. In (3.5) below, we will first derive the solution to the biharmonic problem and then impose the boundary conditions. As introduced in Section 2.2, by substituting the definition of θ given in (2.16) into (3.2), we obtain the explicit expression for the energy:

$$\mathcal{G}(\bar{v}; B_R(0)) = -\frac{1}{2} \sum_{k=1}^K s_k \bar{v}(y^k), \tag{3.3}$$

where K denotes the number of disclinations present in the domain, and each pair (s_k, y^k) represents the Frank angle and the position of the k-th disclination, respectively.

Let us restrict ourselves, for the moment, to the case of a single disclination, K = 1. In this scenario, the differential problem reads

$$\begin{cases} \frac{1-\nu^2}{E}\Delta^2 v = -s\delta_y & \text{in } B_R(0), \\ v = \partial_n v = 0 & \text{on } \partial B_R(0), \end{cases}$$
(3.4)

where $y \in B_R(0)$ represents the position of the single disclination and the associated energy functional is

$$\mathcal{I}^{\theta}(v; B_R(0)) = \mathcal{G}(v; B_R(0)) + s\langle \delta_u, v \rangle,$$

where δ is a Dirac delta centered in y.

The problem in (3.4) can be interpreted as a point source energy version of the *clamped disk problem*, where the source term is represented by a disclination localized at the point $y \in B_R(0)$. The solution \bar{v} can be expressed in terms of the Green's function of the biharmonic operator with clamped boundary conditions, as presented in [45].

Under the assumption that the biharmonic operator Δ^2 is defined as the composition of the Laplacian with itself, i.e., $\Delta^2 = \Delta \Delta$, and by reformulating the problem in polar coordinates, we have that

$$\frac{1}{\rho}\partial_{\rho}(\rho\partial_{\rho}(\frac{1}{\rho}\partial_{\rho}(\rho\partial_{\rho}\bar{v}))) = 0;$$

$$\partial_{\rho}(\frac{1}{\rho}\partial_{\rho}(\rho\partial_{\rho}\bar{v})) = \frac{A}{\rho};$$

$$\partial_{\rho}(\rho\partial_{\rho}\bar{v}) = A\rho\log\rho + B\rho;$$

$$\partial_{\rho}\bar{v} = \frac{A}{4}\rho(\log\rho^{2} - 1) + \frac{B}{2}\rho + \frac{C}{\rho};$$

$$\bar{v} = \tilde{A}\rho^{2}\log\rho^{2} + \tilde{B}\rho^{2} + C\log\rho + D.$$
(3.5)

From this expression, we aim to determine the constants \tilde{A} , \tilde{B} , C, and D by imposing the boundary conditions $v = \partial_n v = 0$ on $\partial B_R(0)$. More precisely, the function $\bar{v} \in H_0^2(\Omega)$ is such that

$$\bar{v}(x) := \begin{cases} \bar{u}(x), & x \in B_R(0) \setminus \{y\}, \\ \bar{w}, & x = y, \end{cases}$$
 (3.6)

where the terms $\bar{u}(x)$ and \bar{w} are explicitly given by:

$$\bar{u}(x) := -\frac{E}{1 - \nu^2} \frac{sR^2}{16\pi} \left[\frac{|x - y|^2}{R^2} \log \left(\frac{|x - y|^2}{R^2} \right) + \left(1 - \frac{|x|^2}{R^2} \right) \left(1 - \frac{|y|^2}{R^2} \right) - \frac{|x - y|^2}{R^2} \log \left(\frac{R^4 - 2R^2x \cdot y + |x|^2|y|^2}{R^4} \right) \right],$$

$$\bar{w} := -\frac{E}{1 - \nu^2} \frac{sR^2}{16\pi} \left(1 - \frac{|y|^2}{R^2} \right)^2.$$

Substituting the expression for $\bar{v}(x)$ into (3.3) yields

$$\mathcal{G}(\bar{v}; B_R(0)) = \frac{E}{1 - \nu^2} \frac{s^2 R^2}{32\pi} \left(1 - \frac{|y|^2}{R^2} \right)^2.$$
 (3.7)

We now generalize to the case where K disclinations are present inside the domain. Exploiting the principle of superposition of effects, the differential problem reads

$$\begin{cases} \frac{1-\nu^2}{E}\Delta^2 v = -\theta_K & \text{in } B_R(0), \\ v = \partial_n v = 0 & \text{on } \partial B_R(0), \end{cases}$$

where θ_K represents the total incompatibility distribution generated by the K defects, each localized at the point $y^k \in B_R(0)$ with Frank angle s_k .

Thanks to the linearity of the biharmonic operator and the boundary conditions, the solution to the problem can be expressed as the sum of the solutions corresponding to single-defect problems. Let \bar{v}_k denote the solution associated with the defect located at y^k , that is:

$$\bar{v}(x) = \sum_{k=1}^{K} \bar{v}_k(x), \quad \text{with} \quad \bar{v}_k(x) := \begin{cases} \bar{u}_k(x), & x \in B_R(0) \setminus \{y^k\}, \\ \bar{w}_k, & x = y^k, \end{cases}$$
(3.8)

where the functions $\bar{u}_k(x)$ and \bar{w}_k are explicitly given by:

$$\bar{u}_k(x) = -Cs_k \left[\frac{|x - y^k|^2}{R^2} \log \left(\frac{|x - y^k|^2}{R^2} \right) + \left(1 - \frac{|x|^2}{R^2} \right) \left(1 - \frac{|y^k|^2}{R^2} \right) - \frac{|x - y^k|^2}{R^2} \log \left(\frac{R^4 - 2R^2x \cdot y^k + |x|^2|y^k|^2}{R^4} \right) \right],$$

$$\bar{w}_k := -Cs_k \left(1 - \frac{|y^k|^2}{R^2} \right)^2,$$

where the constant C is defined as

$$C \coloneqq \frac{ER^2}{16\pi(1-\nu^2)}.\tag{3.9}$$

Substituting the expression for $\bar{v}(x)$ in (3.8) into the energy in (3.3), it follows that

$$\mathcal{G}(\bar{v}; B_R(0)) = -\frac{1}{2} \sum_{k=1}^K s_k \bar{v}(y^k) = -\frac{1}{2} \sum_{k=1}^K \sum_{\ell=1}^K s_k \bar{v}_\ell(y^k) =$$

$$= -\frac{1}{2} \sum_{k=1}^K s_k \bar{v}_k(y^k) - \sum_{k=1}^K \sum_{\ell=k+1}^K s_k \bar{v}_\ell(y^k) =$$

$$= -\frac{1}{2} \sum_{k=1}^K s_k \bar{w}_k - \sum_{k=1}^K \sum_{\ell=k+1}^K s_k \bar{u}_\ell(y^k),$$

which yields a fully explicit formulation of the elastic energy of the system as a function of the positions y^k and intensities s_k of the disclinations. This expression constitutes a fundamental starting point for the study of defect dynamics and their mutual interactions.

At this point, by applying the maximal dissipation criterion, it is possible to derive the dissipative dynamics of the defects by considering the gradient of the energy with respect to the position of each disclination. This leads to the formulation of the following system of ordinary differential equations:

$$\begin{cases} \dot{y}^k(t) = -\lambda_k \nabla_{y^k} \mathcal{G}(\bar{v}, B_R(0)), \\ y^k(0) = y_{k,0}, \end{cases}$$
(3.10)

where λ_k is a positive parameter with units $[\lambda_k] = [s \, kg^{-1}]$.

In the isotropic case where $\lambda_k = \lambda$ for all k, it is possible to perform a nondimensionalization of the problem by introducing the following scaled variables:

$$Y_k = \frac{y^k}{R}$$
 $X = \frac{x}{R}$, $\mathcal{G} = CH$, $T = \frac{\lambda C}{R^2}t$,

where

$$C = \frac{ER^2}{16\pi(1-\nu^2)}$$

is the constant introduced previously in (3.9) and H denotes the nondimensionalized energy.

In the following treatment, unless otherwise specified, the isotropic case will be considered. However, in Section 3.4, two particular anisotropic cases for the disclination dipole problem will be analyzed: the *fixed distance* and the *constrained-center of the dipole* scenarios, for which the corresponding dynamics will be derived.

The nondimensional system describing the evolution of the disclinations thus takes the form:

$$\begin{cases} \dot{Y}_k = -\nabla_{Y_k} H(Y_1, \dots, Y_K), & k = 1, \dots, K; \\ Y_k(0) = Y_{k,0}, & k = 1, \dots, K; \end{cases}$$
(3.11)

where, by a slight abuse of notation, \dot{Y}_k denotes the derivative with respect to the nondimensional time T of the normalized position of the k-th disclination and

$$H(Y_1, \dots, Y_K) = \frac{1}{2} \sum_{k=1}^K s_k^2 (1 - |Y_k|^2)^2 + \sum_{k=1}^K \sum_{\ell=k+1}^K s_k s_\ell (1 - |Y_\ell|^2) (1 - |Y_k|^2)$$

$$+ \sum_{k=1}^K \sum_{\ell=k+1}^K s_k s_\ell |Y_\ell - Y_k|^2 \log \frac{|Y_k - Y_\ell|^2}{|Y_k - Y_\ell|^2 + (1 - |Y_k|^2) (1 - |Y_\ell|^2)}. \tag{3.12}$$

We have thus derived the dynamics of a finite number of disclinations in the domain \mathbb{S}^1 , by employing the maximal dissipation criterion. This leads to the following system of ordinary differential equations

$$\begin{cases} \dot{Y}_k = F_k(Y_1, \dots, Y_K), & k = 1, \dots, K; \\ Y_k(0) = Y_{k,0}, & k = 1, \dots, K, \end{cases}$$
(3.13)

where

$$F_k(Y_1, \dots, Y_K) := F_k^{(1)}(Y_k) + \sum_{\ell=1, \ell \neq k}^K F_{k\ell}^{(2)}(Y_k, Y_\ell) + \sum_{\ell=1, \ell \neq k}^K F_{k\ell}^{(3)}(Y_k, Y_\ell), \quad (3.14)$$

with

$$F_k^{(1)}(Y_k) := 2s_k^2 (1 - |Y_k|^2) Y_k;$$

$$F_{k\ell}^{(2)}(Y_k, Y_\ell) := 2s_k s_\ell \left(1 - \frac{|Y_k - Y_\ell|^2}{|Y_k - Y_\ell|^2 + (1 - |Y_k|^2)(1 - |Y_\ell|^2)} \right) (1 - |Y_\ell|^2) Y_k;$$

$$F_{k\ell}^{(3)}(Y_k, Y_\ell) := 2s_k s_\ell \left[1 - \frac{|Y_k - Y_\ell|^2}{|Y_k - Y_\ell|^2 + (1 - |Y_k|^2)(1 - |Y_\ell|^2)} + \log \left(\frac{|Y_k - Y_\ell|^2}{|Y_k - Y_\ell|^2 + (1 - |Y_k|^2)(1 - |Y_\ell|^2)} \right) \right] (Y_k - Y_\ell).$$

We observe that the Cauchy–Lipschitz (or Picard–Lindelöf) theorem applies to (3.13), ensuring the global existence and uniqueness of the solution.

3.2 An isolated disclination

Following the work in [11], let us now consider the case of a single disclination (K = 1) in the domain, characterized by a Frank angle of magnitude s > 0. In this case, the non-dimensional energy (obtained by (3.7) imposing the rescaled variables) related to a single disclination is

$$H(Y) = \frac{s^2}{2} (1 - |Y|^2)^2$$
(3.15)

and the dynamics reduces to the following differential equation:

$$\begin{cases} \dot{Y} = 2s^2(1 - |Y|^2) Y, \\ Y(0) = Y_0, \end{cases}$$
 (3.16)

where $Y_0 \in \mathbb{S}^1$ represents the initial (nondimensional) position of the defect. To analyze the dynamics, we introduce a polar complex representation:

$$Y(T) = \rho(T)e^{i\phi(T)},$$

where $\rho(T) \in [0,1)$ is the modulus and $\phi(T) \in [0,2\pi)$ is the phase. In these variables, the system separates into the two equations:

$$\begin{cases} \dot{\rho} = 2s^2(1 - \rho^2)\rho, \\ \rho(0) = \rho_0, \end{cases} \begin{cases} \dot{\phi} = 0, \\ \phi(0) = \phi_0. \end{cases}$$
(3.17)

The second system shows that the polar angle ϕ remains constant in time, while the evolution of the radial distance from the center ρ is governed by a logistic equation (for $\rho \neq 0$). The explicit solution to the problem is given by:

$$\rho(T) = \frac{1}{\sqrt{1 + \mu_0 e^{4s^2 T}}}, \qquad \phi(T) = \phi_0, \quad \forall T > 0,$$
 (3.18)

where $\mu_0 = \frac{1 - \rho_0^2}{\rho_0^2}$.

We first observe that the dynamics of the disclination does not depend on the sign of s, but only on its magnitude: positive and negative disclinations evolve identically. From solution (3.18) it follows that:

- if $\rho_0 = 0$, the disclination is initially located at the center of the disk, the solution remains constant over time: $\rho(T) \equiv 0$ for all T > 0. In this case, the defect does not move due to the symmetry of the problem;
- if $\rho_0 \neq 0$, then $\rho(T) \to 1$ as $T \to +\infty$, meaning the disclination is progressively attracted toward the boundary of the domain;
- the attraction towards the boundary is asymptotic: the defect's position approaches |Y(T)| = 1 only as $T \to +\infty$, so no collision with the boundary occurs in finite time;
- The configuration with the disclination centered is unstable: even a small perturbation of ρ_0 leads the trajectory to diverge towards the boundary.

In particular, we can prove the last remark by observing that $\rho(T) = 0$ is a stationary point and

$$\frac{\mathrm{d}}{\mathrm{d}\rho} (2s^2(1-\rho^2)\rho) \bigg|_{\rho=0} = 2s^2(1-3\rho^2) \Big|_{\rho=0} = 2s^2 > 0, \tag{3.19}$$

so we can conclude that $\rho = 0$ is an unstable point.

This simple case reveals a fundamental behavior: in the presence of a single disclination, the energy of the system is minimized when the defect reaches the boundary of the domain. This effect is reflected in the dynamics, which drives the disclination toward the boundary, consistent with the maximal dissipation criterion.

3.3 Radial dipole

The analysis of the dynamics of defects configurations in elastic materials is of fundamental importance for understanding the mechanisms that govern mechanical properties at the microscopic scale. In particular, while the presence of isolated disclinations is theoretically significant, such configurations are energetically unfavorable in practice: a single disclination generates a long-range stress field that results in infinite energy in unbounded domains, or in any case leads to very high energy even in bounded ones [22]. For this reason, the configurations most commonly observed in nature are those in which defects combine into more energetically stable structures. One of the simplest and most relevant among these is the disclination dipole. This configuration is energetically more compact, as the stress fields generated by the two defects tend to cancel each other out at large distances [25, 33, 42].

Let $s_1 = -s_2 =: s > 0$ denote the Frank angle of the dipole of disclinations. The dynamics of the system consisting of two interacting disclinations in a two-dimensional domain is governed by the following system of ordinary differential equations:

$$\begin{cases} \dot{Y}_1 = -\nabla_{Y_1} H(Y_1, Y_2), \\ \dot{Y}_2 = -\nabla_{Y_2} H(Y_1, Y_2), \end{cases}$$
(3.20)

where H denotes the nondimensional energy of the system, which depends on the positions of the two defects and is obtained from (3.12) by imposing K = 2:

$$\begin{split} H(Y_1,Y_2) &= \frac{s^2}{2} \bigg[(1-|Y_1|^2)^2 + (1-|Y_2|^2)^2 \bigg] - s^2 (1-|Y_1|^2) (1-|Y_2|^2) \\ &- s^2 |Y_1 - Y_2|^2 \log \frac{|Y_1 - Y_2|^2}{|Y_1 - Y_2|^2 + (1-|Y_1|^2)(1-|Y_2|^2)} \,. \end{split}$$

We now consider the case where the dipole is arranged radially, meaning that the line connecting the defect positions passes through the center of the disk. We introduce the following quantities.

Definition 3.3.1. We define the **distance** as the length of the segment joining the two defects:

$$h(T) := h(Y_1(T), Y_2(T)) = |Y_1(T) - Y_2(T)|.$$

Definition 3.3.2. We define the **center** of the dipole as the arithmetic mean of the positions of the two disclinations:

$$d(T) := d(Y_1(T), Y_2(T)) = \frac{Y_1(T) + Y_2(T)}{2}.$$

Without loss of generality, we assume that $Y_1 > Y_2$. The positions of the two defects can therefore be rewritten as:

$$Y_1(T) = d(T) + \frac{h(T)}{2}$$
 and $Y_2(T) = d(T) - \frac{h(T)}{2}$.

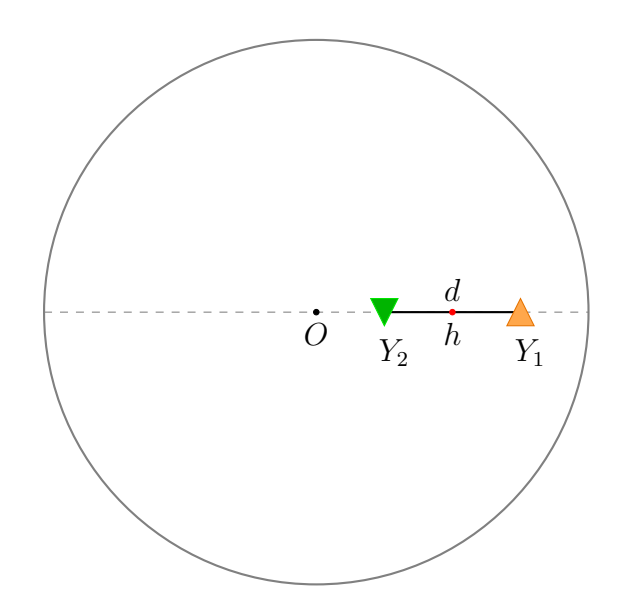


Figure 3.1: A disclination dipole in radial symmetry. The green triangle represents a negative disclination, while the orange one is a positive disclination.

After performing this change of variables and exploiting the symmetry of the decomposition, the problem is now defined in the domain

$$\tilde{\Omega} := \left\{ (h, d) \in (0, 2) \times [0, 1) : 0 < d + \frac{h}{2} \le 1 \right\},$$

instead of the original unit disk. By substituting this representation into the System (3.20), we obtain the following dynamical system for the variables (h, d):

$$\begin{cases}
\dot{h} = F_1 - F_2, \\
h(0) = Y_{1,0} - Y_{2,0} =: h_0,
\end{cases}$$

$$\begin{cases}
\dot{d} = (F_1 + F_2)/2, \\
d(0) = (Y_{1,0} + Y_{2,0})/2 =: d_0,
\end{cases}$$
(3.21)

where h_0 , d_0 are the initial conditions for the distance of the defects and the center of the dipole and they are obtained from $Y_{1,0}$, $Y_{2,0}$ the initial positions of the defects. In (3.21), we have posed

$$F_1 := F_1(h, d) = 2s^2 \left[2h \log \left(\frac{4h}{h^2 + 4 - 4d^2} \right) - h \left(\frac{4h}{h^2 + 4 - 4d^2} \right)^2 + h + \left(d + \frac{h}{2} \right) \left(\frac{h}{2} + d - 1 \right) + \left(d + \frac{h}{2} \right) \left(-d^2 + dh - \frac{h^2}{4} + 1 \right) \cdot \left(\frac{-16d^4 + 8d^2h^2 + 32d^2 - h^4 + 8h^2 - 16}{(h^2 + 4 - 4d^2)^2} \right) \right]$$

and

$$F_2 := F_2(h, d) = -2s^2 \left[2h \log \left(\frac{4h}{h^2 + 4 - 4d^2} \right) + h \left(\frac{4h}{h^2 + 4 - 4d^2} \right)^2 - h \right]$$
$$- \left(d - \frac{h}{2} \right) \left(\frac{h}{2} - d + 1 \right) - \left(d - \frac{h}{2} \right) \left(-d^2 + dh + \frac{h^2}{4} - 1 \right) \cdot \left(\frac{-16d^4 + 8d^2h^2 + 32d^2 - h^4 + 8h^2 - 16}{(h^2 + 4 - 4d^2)^2} \right) \right]$$

For the sake of clarity, we introduce:

$$f(h,d) := F_1 - F_2$$

$$= 4s^2 h \left[2\log\left(\frac{4h}{h^2 - 4d^2 + 4}\right) - \frac{2h^2d^2 + h^2 - 8d^4 + 12d^2 - 4}{h^2 - 4d^2 + 4} \right]$$
(3.22)

as the driving force of the distance between the defects and

$$g(h,d) := \frac{F_1 + F_2}{2} = -\frac{2s^2h^2d(h^2 - 4d^2)}{h^2 - 4d^2 + 4}$$
(3.23)

as the driving force of the center of the dipole.

System (3.21) governs the time evolution of the dipole configuration within the domain. A qualitative analysis of its solutions reveals whether the defects tend to migrate toward the boundary or remain in symmetric configurations, depending on the initial data and the geometric features of the setting. Figure 3.2 displays the plots of the two driving forces. In particular, Figure 3.2a illustrates the behavior of the forcing term associated with the evolution of the distance h between the disclinations. A negative value of this function corresponds to an attractive interaction (the distance h decreases), while a positive value indicates repulsion (the defects move apart). Zero values identify configurations where the distance remains stationary. Similarly, Figure 3.2b shows the driving force governing the evolution of the center of the dipole d. When this force is negative, the dipole moves toward the center of the domain, while a positive value indicates a drift toward the boundary. Again, vanishing values correspond to stationary positions of the center of the dipole.

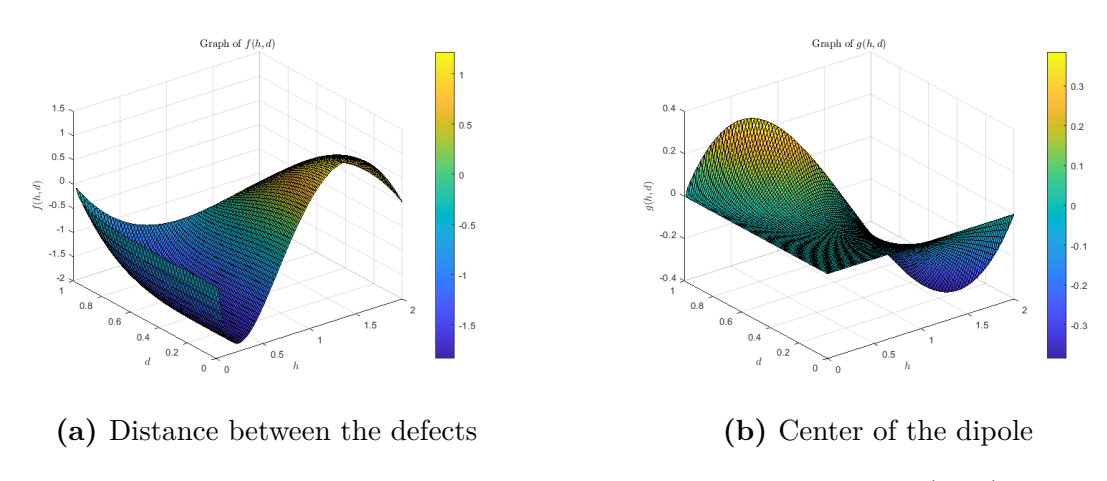
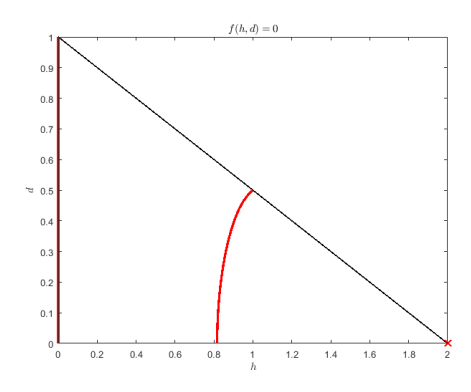


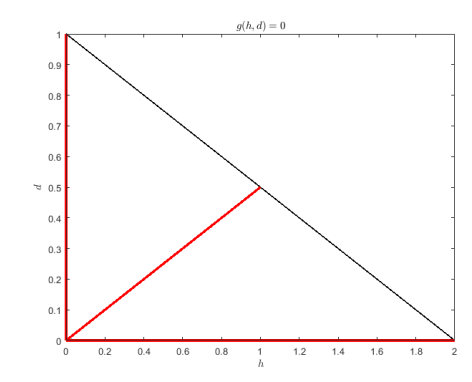
Figure 3.2: Behavior of the forcing functions of System (3.21).

We now proceed to analyze the dynamics of the system by identifying the zeroes of the functions f(h, d) and g(h, d). Setting f(h, d) = 0, we find that the trivial condition h = 0 is a solution for all d, as well as the more involved condition

$$2\log\left(\frac{4h}{h^2+4-4d^2}\right) - \frac{2h^2d^2+h^2-8d^4+12d^2-4}{h^2+4-4d^2} = 0.$$

Similarly, solving g(h, d) = 0, we obtain the solutions h = 0 for all d, d = 0 for all h, and h = 2d. Figure 3.3 displays the zero-level curves of both functions. The intersections of these curves indicate stationary configurations for the dipole.





(a) Distance between the defects

(b) Center of the dipole

Figure 3.3: Zeroes of f(h, d) and g(h, d).

We are interested in identifying the equilibrium points (h^*, d^*) of the dynamical system (3.21), namely the stationary configurations of the disclination dipole. These are the points in the domain $\tilde{\Omega}$ such that both driving forces vanish:

$$f(h^*, d^*) = 0$$
 and $q(h^*, d^*) = 0$.

We identify and characterize the following stationary points.

Lemma 3.3.1 (Stationary points). The following hold:

- 1. the point $E_1 = (2,0)$ is an asymptotically stable equilibrium;
- 2. the point $E_2 = (1, \frac{1}{2})$ is an unstable equilibrium;
- 3. the point $E_3 = (h^*, 0)$, with $h^* \approx 0.8$, is an unstable equilibrium (the same equilibrium point analyze in [11]);
- 4. the set $E_4 = \{(h, d) \in \Omega : h = 0\}$ is an attracting set.

Proof. To analyze the stability of E_1, E_2, E_3 , we compute the Jacobian matrix of the system:

$$J(h,d) = \begin{bmatrix} \partial_h f(h,d) & \partial_d f(h,d) \\ \partial_h g(h,d) & \partial_d g(h,d) \end{bmatrix},$$

with

$$\partial_h f(h, d) = 4 s^2 \left[2 \log \left(\frac{4 h}{h^2 + 4 - 4 d^2} \right) - \frac{32 d^6 - 16 d^4 (h^2 + 7) + 2 d^2 (h^4 + 64) + 3 h^4 + 16 h^2 - 48}{(h^2 - 4 d^2 + 4)^2} \right];$$

$$\partial_{d}f(h,d) = -\frac{16 d h s^{2} (16 d^{4} - 8 d^{2} h^{2} - 16 d^{2} + h^{4} + 8 h^{2})}{(-4 d^{2} + h^{2} + 4)^{2}};$$

$$\partial_{h}g(h,d) = -\frac{4 d h s^{2} (16 d^{4} - 8 d^{2} h^{2} - 16 d^{2} + h^{4} + 8 h^{2})}{(-4 d^{2} + h^{2} + 4)^{2}};$$

$$\partial_{d}g(h,d) = -\frac{2 h^{2} s^{2} (16 d^{4} - 8 d^{2} h^{2} - 48 d^{2} + h^{4} + 4 h^{2})}{(-4 d^{2} + h^{2} + 4)^{2}}.$$

Evaluating the Jacobian at E_1 and computing the eigenvalues, we find $\lambda_{E_1}^{(1)} = \lambda_{E_1}^{(2)} = -4$: both are negative and the equilibrium is asymptotically stable. In the same fashion, we can also prove that the points the eigenvalues related to E_2 are $\lambda_{E_2}^{(1)} = 2$, $\lambda_{E_2}^{(2)} = 0$ and those related to E_3 are $\lambda_{E_3}^{(1)} \approx 3.75$, $\lambda_{E_3}^{(2)} = -0.19$: because of the presence of eigenvalues with a positive real part, we can conclude that both E_2 and E_3 are unstable equilibrium configurations.

Let us consider the case h = 0. We observe that it is possible to extend for continuity f in h = 0 as follow:

$$f(h,d) := \begin{cases} 4s^2h \left[2\log\left(\frac{4h}{h^2 - 4d^2 + 4}\right) - \frac{2h^2d^2 + h^2 - 8d^4 + 12d^2 - 4}{h^2 - 4d^2 + 4} \right] & \text{if } h \neq 0; \\ 0 & \text{if } h = 0. \end{cases}$$

We observe that the qualitative behavior of the system can be studied by dividing the analysis into two distinct regions: one where $\dot{h} < 0$ and $\dot{d} < 0$, and another where $\dot{h} < 0$ and $\dot{d} > 0$. In both cases, the functions h and d exhibit monotonic behavior: specifically, h is strictly decreasing, while d is decreasing in the first region and increasing in the second. Moreover, both variables are bounded, since $h(T) \in [0,2)$ and $d(T) \in [0,1)$. Therefore, we can assert the existence of limits as $T \to +\infty$, denoted by:

$$\lim_{T \to +\infty} h(T) = h_{\infty} \in [0,2), \qquad \lim_{T \to +\infty} d(T) = d_{\infty} \in [0,1).$$

Given that the forcing terms f and g of the system are continuous with respect to h and d, it follows that:

$$\begin{cases} \lim_{T \to +\infty} \dot{h}(T) = f(h_{\infty}, d_{\infty}) \in \mathbb{R}, \\ \lim_{T \to +\infty} \dot{d}(T) = g(h_{\infty}, d_{\infty}) \in \mathbb{R}. \end{cases}$$

If $(h_{\infty}, d_{\infty}) \in \text{dom}(f) \cap \text{dom}(g)$, then by the asymptotic stability theorem (or under the assumption of asymptotic regularity), we obtain:

$$\begin{cases} \dot{h}(+\infty) = f(h_{\infty}, d_{\infty}) = \hat{h}_{\infty}, \\ \dot{d}(+\infty) = g(h_{\infty}, d_{\infty}) = \hat{d}_{\infty}. \end{cases}$$

However, since both h and d converge, we must have:

$$\begin{cases} f(h_{\infty}, d_{\infty}) = 0, \\ g(h_{\infty}, d_{\infty}) = 0, \end{cases}$$

so the point (h_{∞}, d_{∞}) is a stationary point of the system. If we further assume that the nullclines satisfy:

$$\begin{cases} f(h,d) = 0 \\ g(h,d) = 0 \end{cases} \iff \begin{cases} h = 0 \\ d = \bar{d} \in [0,1) \end{cases}$$

then the only possible equilibrium point as $T \to +\infty$ is

$$(h_{\infty}, d_{\infty}) = (0, \bar{d}), \quad \text{for some } \bar{d} \in [0, 1).$$

Remark 3.3.1. The equilibrium point $E_2 = (1,0.5)$ represents a limiting case of the model, where one defect is located at the center of the domain and the other lies exactly on the boundary. In this configuration, the defect at the center does not feel the influence of the one at the boundary, and due to symmetry, it remains stationary. Consequently, this case can be interpreted as a limiting situation in which the defect at the center behaves as an isolated defect (as demonstrated in Section 3.3.4).

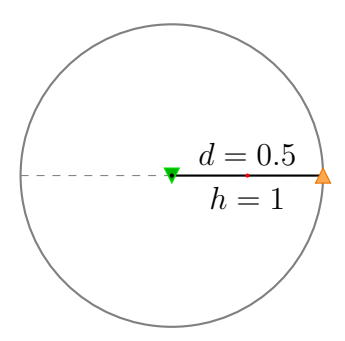


Figure 3.4: Representation of the equilibrium point $E_2 = (1, \frac{1}{2})$. In this scenario the positive disclination (orange triangle) lies on the boundary of the domain, while the negative one (green triangle) is sitting at the center of the disk.

3.3.1 Numerical simulations

It is not possible to analytically solve System (3.21), so to gain insight into the dynamics of the dipole an explicit Euler method with a fixed timestep was implemented in MATLAB R2023b. This problem is ill-conditioned and also the stiff solvers natively implemented in MATLAB (such as ode23s and ode23t [47]) produce solutions that do not align with expected results. Specifically, using these solvers, it is possible to observe oscillatory motions where the two defects overlap and exchange positions (see Figure 3.5).

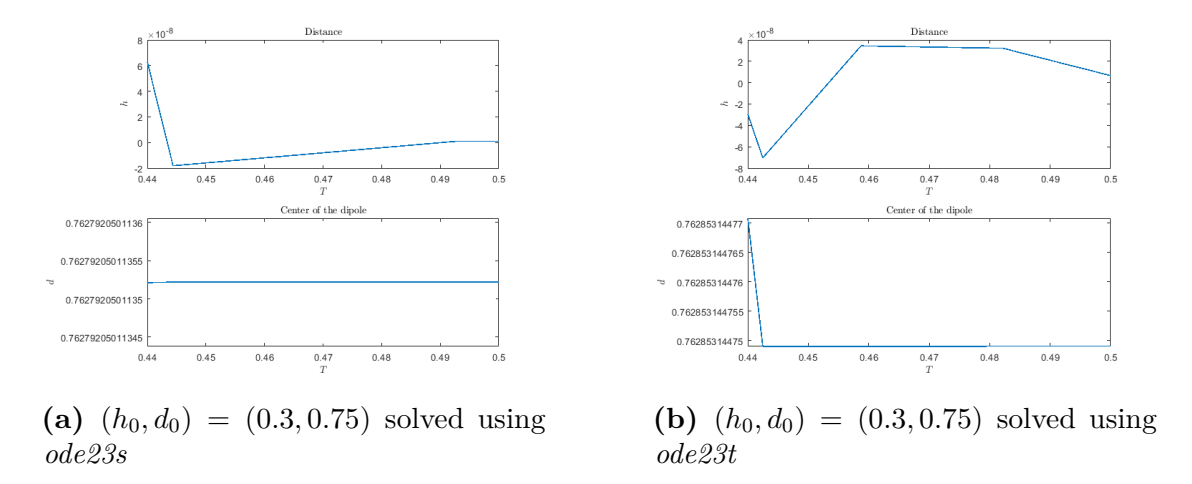


Figure 3.5: Details of the interaction between defects in the presence of numerical errors using different stiff solvers in Matlab.

As demonstrated in [11, Section 4.2] for a symmetric configuration and in Sections 3.3.2 and 3.3.3 below, this behavior of defects is prohibited: two defects must asymptotically approach each other, but they cannot overlap in finite time.

To gain a more complete understanding of the dynamics, we proceeded by solving the problem at various points in the domain and analyzing the obtained results (excluding d=0 which has been already studied in [11] and h=0 which is a nonphysical configuration).

Figure 3.6 shows the results of the analysis performed over a time interval [0,20]. The obtained results are then classified as follows:

- The filled square represents the behavior of the distance by comparing the initial and final conditions. Specifically, if the color is yellow, the defects are converging on the boundary of the domain $(h \to 0, d \to 1)$; if the color is green, the defects are converging $(h \to 0)$ at some point $\bar{d} \in [0, 1)$; if the color is blue, the defects are diverging to opposite edges of the domain $(h \to 2, d \to 0)$. The triangle represents the stationary points.
- The border of the square represents the behavior of the center of the dipole by comparing the initial d_0 and final conditions \bar{d} . Specifically, when the border is blue, the final position of the center of the dipole is expected to have increased

compared to the initial position $(\bar{d} \in (d_0,1))$; when it is red, the center of the dipole is expected to have decreased $(\bar{d} \in [0,d_0))$; when it is green, no change is expected $(\bar{d} = d_0)$.

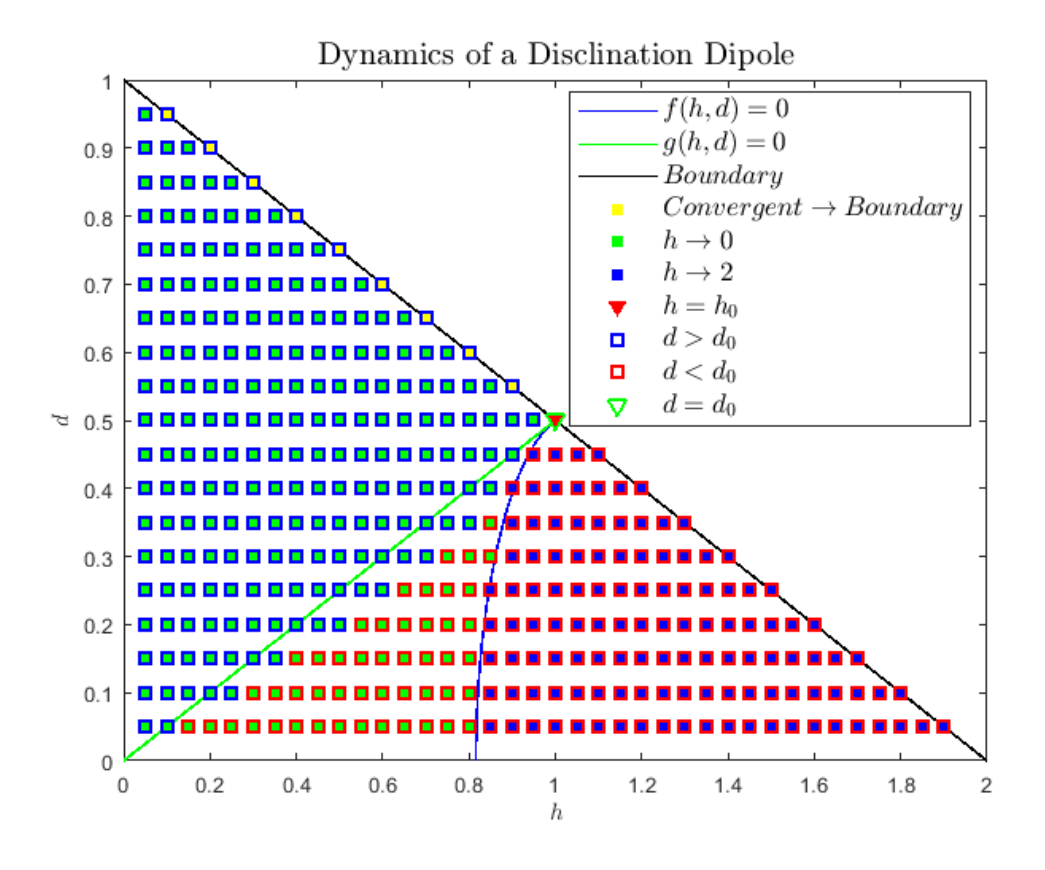


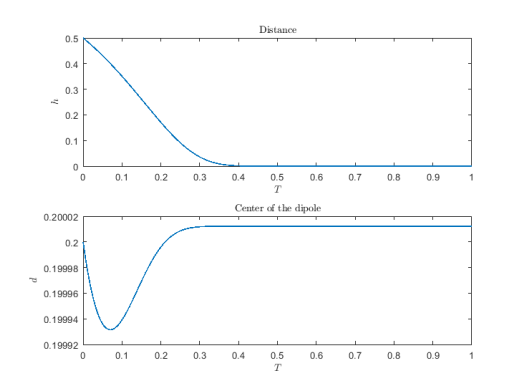
Figure 3.6: Scheme of the dynamics of a dipole of disclinations.

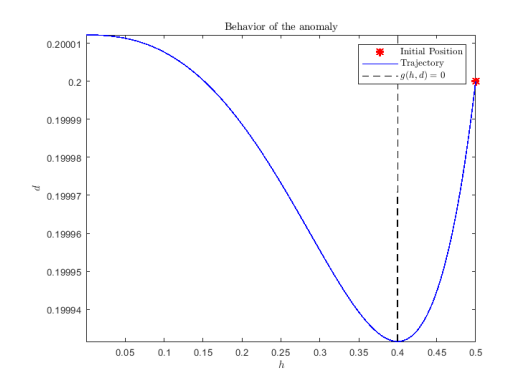
As can be seen graphically, the three regions defined by the zeros of f and g can be characterized as follows.

- Region 1: $\dot{h} < 0$ and $\dot{d} > 0$, which corresponds to the case where the two defects converge and the center of the dipole shifts towards the boundary of the domain. This corresponds to the squares with a blue border.
- Region 2: h < 0 and d < 0, which corresponds to the case where the defects converge and the center of the dipole shifts towards the center of the domain. This corresponds to the squares with a red border.
- Region 3: $\dot{h} > 0$ and $\dot{d} < 0$, which corresponds to the case where the defects diverge to opposite edges of the domain and the center of the dipole shifts towards the center. This corresponds to the squares with a red border.

From this summary scheme, some observations can be made. If we consider the cases analyzed along the hypotenuse of the triangular domain $\tilde{\Omega}$, we examine the problems where one defect is located at the boundary of the domain and the other along the radius. Consistently with the stationary limiting case previously observed, the non-boundary defect tends to behave as an isolated defect and tends to move toward the domain boundary, as proved analytically in Section 3.3.2. It is important to note that, contrary to the initial hypotheses made, the dynamics of the dipole exhibit an anomaly. As it can also be seen graphically, just below the curve representing the zeros of g(h,d), the border of the squares is blue instead of red.

To further investigate, Figure 3.7a shows the graph of the solution with $(h_0, d_0) = (\frac{1}{2}, \frac{1}{5})$ as starting point.





- (a) Detailed of the dynamics of a dipole $(h_0, d_0) = (\frac{1}{2}, \frac{1}{5})$
- **(b)** Details of the anomaly in $(h_0, d_0) = (\frac{1}{2}, \frac{1}{5})$

Figure 3.7: Details of the anomaly near g(h, d) = 0.

As it can be observed, initially the center of the dipole decreases, consistently with expectations, but then tends to increase before stabilizing at a position higher than the initial one. This indicates that the dynamics of the distance dominates the dynamics of the center of the dipole, leading to a change in sign in the description of the motion of the center of the dipole.

Let us consider $[0, \bar{T}]$ as the integral time, with $\bar{T} > 0$ (referring to our simulation, $\bar{T} = 20$); $n \in \{0, ..., N\}$ with $N \in \mathbb{N} \setminus \{0\}$. We define

$$\delta T := \frac{T}{N}$$
 and $T_n := n \, \delta T = \frac{n}{N} \, T$,

and we consider

$$h^n := h(T_n), \qquad d^n := d(T_n).$$

It is possible to better understand this behavior by analyzing step-by-step the explicit Euler methods

$$\begin{cases} h^{n+1} = h^n + \delta T f(h^n, d^n) \\ d^{n+1} = d^n + \delta T g(h^n, d^n). \end{cases}$$

Step one:

$$h^{1} = h^{0} + \delta T \underbrace{f(h^{0}, d^{0})}_{<0} < h^{0}$$
$$d^{1} = d^{0} + \delta T \underbrace{g(h^{0}, d^{0})}_{<0} < d^{0},$$

we can determinate the sign of f, g, because we chose h^0, d^0 to be such that $\dot{h} < 0$ and $\dot{d} < 0$.

Step two:

$$h^{2} = h^{1} + \delta T f(h^{1}, d^{1}) < h^{1}$$
$$d^{2} = d^{1} + \delta T \underbrace{g(h^{1}, d^{1})}_{\text{undetermined sign}}$$

we can say that the sign of $f(h^1, d^1)$ is still negative, because $h^1 < h^0$ and $d^1 < d^0$, but we can not define the sign of $g(h^1, d^1)$ without knowing the exact value of h^1 and d^1 . In particular, if $h^1 \to 0$ is faster then d^1 , then $g(h^1, d^1) > 0$. As it can be seen in Figure 3.7b starting from $(h_0, d_0) = (\frac{1}{2}, \frac{1}{5})$, \dot{h} is faster than \dot{d} , so that \dot{d} became positive and it generates the anomaly.

We now analyze the behavior of the dipole within the previously defined Region 1, 2, 3. Our goal is to identify suitable upper and lower bounds of the dynamics in order to obtain estimates on the evolution of the dipole. To this end, we recall the following preliminary lemma, which will be instrumental in our analysis.

Lemma 3.3.2 (Preliminary lemma). Let us consider the Cauchy problem

$$\begin{cases} \dot{x}(t) = \psi(t, x(t)), \\ x(0) = x_0, \end{cases} \quad x(t) \in \mathbb{R}^n,$$

and suppose that there exist continuous functions $\zeta_1, \zeta_2 : \mathbb{R} \times \mathbb{R}^n \to \mathbb{R}$ such that

$$\zeta_1(t,x) \leq \psi(t,x) \leq \zeta_2(t,x)$$
 componentwise for all $(t,x) \in \mathbb{R} \times \mathbb{R}^n$.

Then, the solutions $x_1(t)$ and $x_2(t)$ of the Cauchy problems

$$\dot{x}_1(t) = \zeta_1(t, x_1(t)), \qquad \dot{x}_2(t) = \zeta_2(t, x_2(t)), \qquad x_1(0) = x_2(0) = x_0,$$

satisfy the componentwise estimate

$$x_1(t) \le x(t) \le x_2(t)$$
 for all $t \ge 0$.

Proof. Let us consider the Cauchy problem for the system:

$$\begin{cases} \dot{x}(t) = \psi(t, x(t)), \\ x(0) = x_0. \end{cases}$$

We are given that there exist continuous functions $\zeta_1, \zeta_2 : \mathbb{R} \times \mathbb{R}^n \to \mathbb{R}$ such that

$$\zeta_1(t,x) \le \psi(t,x) \le \zeta_2(t,x)$$
 componentwise for all $(t,x) \in \mathbb{R} \times \mathbb{R}^n$.

To prove the lemma, we first note that the functions $\zeta_1(t,x)$ and $\zeta_2(t,x)$ are continuous, and therefore the Cauchy problems

$$\dot{x}_1(t) = \zeta_1(t, x_1(t)), \quad \dot{x}_2(t) = \zeta_2(t, x_2(t)), \quad x_1(0) = x_2(0) = x_0$$

have unique solutions $x_1(t)$ and $x_2(t)$, respectively, for all $t \ge 0$. Now, consider the difference between the solutions of the two systems. Let us define the difference $y(t) = x_2(t) - x_1(t)$. Then, we have the system:

$$\dot{y}(t) = \dot{x}_2(t) - \dot{x}_1(t) = \zeta_2(t, x_2(t)) - \zeta_1(t, x_1(t)).$$

Since $\zeta_1(t,x) \leq \psi(t,x) \leq \zeta_2(t,x)$ componentwise, we deduce that

$$\dot{y}(t) = \zeta_2(t, x_2(t)) - \zeta_1(t, x_1(t)) \ge 0.$$

Thus, the solution y(t) is non-decreasing. Since $y(0) = x_2(0) - x_1(0) = 0$, it follows that $y(t) \ge 0$ for all $t \ge 0$. Therefore, we obtain the componentwise estimate

$$x_1(t) \le x_2(t)$$
 for all $t \ge 0$.

In particular, since $x_1(t)$ and $x_2(t)$ are solutions of the Cauchy problems with the same initial condition x_0 , we have

$$x_1(t) \le x(t) \le x_2(t)$$
, for all $t \ge 0$.

3.3.2 Region 1: boundary behaviour

Inside Region 1, we have $\dot{h} < 0$ and $\dot{d} > 0$, which means that we expect the dipole to collapse and its center to move towards the boundary. Referring to Figure 3.6, we analyze the case with the squares with blue borders. Consequently, inside this region, we have the following conditions hold:

$$0 < h(T) \le h_0 \le 1$$
 and $0 \le d_0 \le d(T) \le 1$, for all $T > 0$.

In particular, we can define Region 1 as

$$\Omega_1 := \left\{ (h, d) \in (0, 1] \times [0, 1) : d + \frac{h}{2} < 1 \text{ and } d - \frac{h}{2} < 0 \right\} \cap \tilde{\Omega}.$$

From Lemma 3.3.1, we know that $h \to 0$ and we wish to investigate the rate at which this occurs. More specifically, we are interested in determining whether there exists a time $\tilde{T} > 0$ such that $h(\tilde{T}) = 0$ or if $h \to 0$ as $T \to +\infty$. We would also like to prove some regularity properties of h. Similarly, we are interested in understanding whether there exists a value $d > d_0$ such that $d \to d$ or if $d \to 1$ as $T \to +\infty$. To answer these questions, we will proceed by defining appropriate upper and lower bounds for both f and g, which, together with Lemma 3.3.2, will allow us to extract the desired information.

Theorem 3.3.1 (Bounds for f and g in Ω_1). Consider $(h, d) \in \Omega_1$, then there exist functions $h_l^{(1)}, h_u^{(1)} : \mathbb{R}^+ \to \mathbb{R}$ such that

$$h_l^{(1)}(T) \le h(T) \le h_u^{(1)}(T), \quad \text{for all } T > 0.$$

In particular, $h_l^{(1)}$ is defined by

$$h_l^{(1)}(T) = C_1 \exp\left(-C_2 \exp(8s^2 T)\right),$$

where $C_1 := \frac{h_0^2 + 4 - 4d_0^2}{4} > 0$ and $C_2 = \log(C_1/h_0) > 0$, while $h_u^{(1)}$ is the solution to

$$\dot{h} = 8s^2 h \log \left(\frac{h}{1 - d^2}\right).$$

There exist functions $d_l^{(1)}, d_u^{(1)} : \mathbb{R}^+ \to \mathbb{R}$ such that

$$d_l^{(1)}(T) \le d(T) \le d_u^{(1)}(T)$$
 for all $T > 0$.

In particular, $d_l^{(1)}$ is the solution to

$$\log\left(\frac{d}{d_0}\right) - \frac{2}{h_0^2}\log\left(\frac{d_0}{d}\left|\frac{h_0^2 - 4d^2}{h_0 - 4d_0^2}\right|\right) = -2s^2 \int_0^T h(t)^2 dt,$$

while $d_u^{(1)}$ is the solution to

$$2\log\left(\frac{d}{d_0}\right) + \frac{1}{d^2} - \frac{1}{d_0^2} = -4s^2 \int_0^T h(t)^2 dt.$$

Proof. First, consider

$$f(h,d) = \underbrace{8s^2h\log\left(\frac{4h}{h^2 + 4 - 4d^2}\right)}_{f_1(h,d)} + \underbrace{\frac{-4hs^2}{h^2 + 4 - 4d^2}(2h^2d^2 + h^2 - 8d^4 + 12d^2 - 4)}_{f_2(h,d)}.$$

For $h \to 0$, $f_2(h, d) \sim o(h)$ for all d, thus we can neglect it. We now estimate f_1 as follows:

$$4(1-d^{2}) \leq h^{2} + 4 - 4d^{2} \leq h_{0}^{2} + 4 - 4d_{0}^{2},$$

$$\frac{1}{h_{0}^{2} + 4 - 4d_{0}^{2}} \leq \frac{1}{h^{2} + 4 - 4d^{2}} \leq \frac{1}{4(1-d^{2})},$$

$$\frac{4h}{h_{0}^{2} + 4 - 4d_{0}^{2}} \leq \frac{4h}{h^{2} + 4 - 4d^{2}} \leq \frac{h}{1-d^{2}},$$

$$\log\left(\frac{4h}{h_{0}^{2} + 4 - 4d_{0}^{2}}\right) \leq \log\left(\frac{4h}{h^{2} + 4 - 4d^{2}}\right) \leq \log\left(\frac{h}{1-d^{2}}\right),$$

$$8s^{2}h\log\left(\frac{4h}{h_{0}^{2} + 4 - 4d_{0}^{2}}\right) \leq 8s^{2}h\log\left(\frac{4h}{h^{2} + 4 - 4d^{2}}\right) \leq 8s^{2}h\log\left(\frac{h}{1-d^{2}}\right).$$

$$(3.25)$$

From Lemma 3.3.2 it follows that exist $h_l^{(1)}, h_u^{(1)}: \mathbb{R}^+ \to \mathbb{R}$ such that

• $h_l^{(1)}$ is the solution to the problem $\dot{h} = 8s^2h\log\left(\frac{4h}{h_0^2+4-4d_0^2}\right)$:

$$h_l^{(1)}(T) = C_1 \exp\left(-C_2 \exp(8s^2T)\right),$$

with $C_1 := \frac{h_0^2 + 4 - 4d_0^2}{4} > 0$ and $C_2 = \log(C_1/h_0) > 0$;

• $h_u^{(1)}$ is the solution to the problem $\dot{h} = 8s^2 h \log \left(\frac{h}{1-d^2}\right)$.

Regarding \dot{d} , using (3.24), we obtain the following upper and lower estimates:

$$\frac{-d^2}{1 - d^2} \le \frac{h^2 - 4d^2}{h^2 + 4 - 4d^2} \le \frac{h_0^2 - 4d^2}{h_0^2 + 4 - 4d^2} \le 0,$$
$$\frac{-2d^3h^2}{1 - d^2} \le 2h^2d\frac{h^2 - 4d^2}{h^2 + 4 - 4d^2} \le 2h^2d\frac{h_0^2 - 4d^2}{h_0^2 + 4 - 4d^2} \le 0.$$

Thus, it follows that

$$-2s^{2}h^{2}d\frac{h_{0}^{2}-4d^{2}}{h_{0}^{2}-4d^{2}+4} \le -2s^{2}h^{2}d\frac{h^{2}-4d^{2}}{h^{2}-4d^{2}+4} \le s^{2}h^{2}\frac{2d^{3}}{1-d^{2}}.$$
 (3.26)

From Lemma 3.3.2 it follows that there exist $d_l^{(1)}, d_u^{(1)}: \mathbb{R}^+ \to \mathbb{R}$ such that

$$d_l^{(1)}: \qquad \log\left(\frac{d}{d_0}\right) - \frac{2}{h_0^2}\log\left(\frac{d_0}{d}\left|\frac{h_0^2 - 4d^2}{h_0^2 - 4d_0^2}\right|\right) = -2s^2 \int_0^T h(t)^2 dt,$$

$$d_u^{(1)}: \qquad 2\log\left(\frac{d}{d_0}\right) + \frac{1}{d^2} - \frac{1}{d_0^2} = -4s^2 \int_0^T h(t)^2 dt.$$

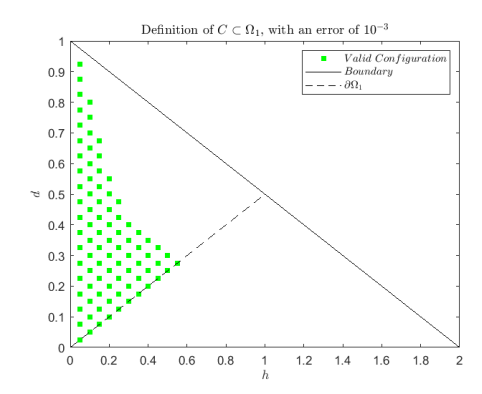
Corollary 3.3.1 (Collision time in Ω_1). In Ω_1 , $h \to 0$ as $T \to \infty$.

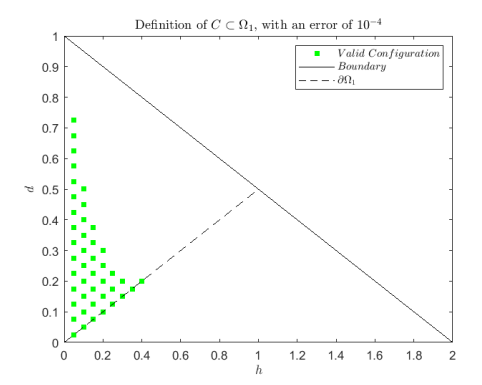
Proof. From the estimates in Theorem 3.3.2, we know that $h_l^{(1)} \to 0$ as $T \to +\infty$. Hence, from Lemma 3.3.1 we know that in this region $h \to 0$, so we can conclude, by comparison, that $h \to 0$ as $T \to +\infty$.

Remark 3.3.2. We can observe that the dynamics of d is proportional to h^2 , and therefore, as $h \to 0$, we have $\dot{d} \sim o(h^2)$, which allows us to assume that d can be approximated as constant $(d(T) = d_0$, for every T > 0).

Definition 3.3.3. Let $C \subseteq \Omega_1$ be the region where the Remark 3.3.2 holds.

We define $C \subseteq \Omega_1$ computationally by solving the problem point by point and selecting those that have an error below a certain low threshold, which we can then estimate as good candidates. The result, after setting a threshold of 10^{-3} and 10^{-4} , is shown in Figure 3.8.





- (a) Considering an error threshold of 10^{-3} .
- (b) Considering an error threshold of 10^{-4} .

Figure 3.8: Numerical definition of $C \subseteq \Omega_1$ based on different error threshold.

Proposition 3.3.1 (Regularity of h in Ω_1). Inside C, as $h_0 \ll 1$, we can state that $h \in L^2(\mathbb{R}^+)$.

Proof. In C we can assume $d(T) \approx d_0$, so from (3.25), we can estimate \dot{h} as

$$8s^{2}h\log\left(\frac{4h}{h_{0}^{2}+4-4d_{0}^{2}}\right) \leq \dot{h} \leq 8s^{2}h\log\left(\frac{h}{1-d_{0}^{2}}\right);$$

since we are assuming that $h_0 \ll 1$, we can neglect it in the left-hand side and obtain that

$$\dot{h} = 8s^2 h \log \left(\frac{h}{1 - d_0^2}\right),\,$$

which can be integrated explicitly, thus we can conclude that

$$h(T) = (1 - d_0^2) \exp\left(\log\left(\frac{h_0}{1 - d_0^2}\right) \exp(8s^2T)\right).$$
 (3.27)

When (3.27) is squared and integrated, this yields

$$\int_0^T h^2(t) dt = \frac{C_1^2}{8} \left(\text{Ei} \left(-2 C_2 \exp(8s^2 T) \right) - \text{Ei} \left(-2 C_2 \right) \right), \tag{3.28}$$

where $C_1 = 1 - d_0^2$ and $C_2 = \log(C1/h_0)$. Here, Ei(·) represents the exponential integral function, defined as:

$$\mathrm{Ei}(x) = -\int_{-x}^{\infty} \frac{e^{-t}}{t} \mathrm{d}t.$$

In particular,

$$\operatorname{Ei}\left(-2\log\left(\frac{1-d_0^2}{h_0}\right)\right) < +\infty,$$

whereas, for $T \to +\infty$, we have:

$$\lim_{T \to +\infty} \operatorname{Ei}\left(-2\log\left(\frac{1 - d_0^2}{h_0}\right) \exp(8s^2T)\right) = 0.$$

Therefore, (3.28) is finite as $T \to +\infty$ and we conclude that $h \in L^2(\mathbb{R}^+)$.

Corollary 3.3.2 (Behavior of d when $T \to +\infty$). In C, we can state that there exist $d_{l,\infty}, d_{u,\infty}$ such that

$$d_{l,\infty} < d(T) < d_{u,\infty}$$
 as $T \to +\infty$.

Proof. Since in C we know an explicit formula for h, we can substitute it into the implicit formulas of the lower and upper bounds from Theorem 3.3.1 and take the limit as $T \to +\infty$. This leads to the determination of $d_{l,\infty}$ and $d_{u,\infty}$.

Limit case

Let us now analytically justify the behavior of defects as $h \to 0$ and $d \to 1$, which corresponds to the case with the full yellow square in Figure 3.6.

Proposition 3.3.2 (Boundary behavior in Ω_1). Consider $(h, d) \in \Omega_1$; when $h \to 0$ and $d \to 1$, the defect $Y_2 = d - \frac{h}{2}$ behaves as an isolated disclination.

Proof. First, we make the following ansatz for $\kappa \to 0$:

$$h(T) = \kappa h_1(T)$$
$$d(T) = 1 + \kappa d_1(T)$$

with $h_1(T) \in (0, \infty)$ and $d_1(T) \in (-\infty, 0)$. We substitute h and d into (3.21) as follow.

$$\begin{split} \kappa \, \dot{h_1} &= \dot{h} = 4\kappa \, s^2 h_1 \bigg[2 \log \bigg(\frac{4\kappa \, h_1}{\kappa^2 \, h_1^2 + 4 - 4(1 + \kappa \, d_1)^2} \bigg) + \\ &- \frac{2\kappa \, h_1^2 (1 + \kappa \, d_1)^2 + \kappa^2 h_1^2 - 8(1 + \kappa \, d_1)^4 + 12(1 + \kappa \, d_1)^2 - 4}{\kappa^2 h_1^2 + 4 - 4(1 + \kappa \, d_1)^2} \bigg], \end{split}$$

by simplifying κ

$$\dot{h}_1 = 4 s^2 h_1 \left[2 \log \left(\frac{4 h_1}{\kappa h_1^2 + 4\kappa d_1^2 + 8 d_1} \right) + \frac{2\kappa h_1^2 (1 + \kappa d_1)^2 + \kappa^2 h_1^2 - 8(1 + \kappa d_1)^4 + 12(1 + \kappa d_1)^2 - 4}{\kappa^2 h_1^2 + 4\kappa^2 d_1^2 + 8\kappa d_1} \right],$$

as $\kappa \to 0$, we obtain

$$\dot{h_1} = 8s^2 h_1 \log \left(-\frac{h_1}{2d_1} \right) - 4s^2 h_1.$$

Similarly,

$$\kappa \, \dot{d}_1 = \dot{d} = -2s^2 \kappa^2 \, h_1^2 (1 + \kappa \, d_1) \frac{\kappa^2 h_1^2 + 4\kappa^2 \, d_1^2 + 8\kappa \, d_1 + 4}{\kappa^2 h_1^2 + 4\kappa^2 \, d_1^2 + 8\kappa \, d_1},$$

by simplifying κ

$$\dot{d}_1 = -2s^2 h_1^2 (1 + \kappa d_1) \frac{\kappa^2 h_1^2 + 4\kappa^2 d_1^2 + 8\kappa d_1 + 4}{\kappa h_1^2 + 4\kappa d_1^2 + 8d_1},$$

and as $\kappa \to 0$, we obtain

$$\dot{d}_1 = -s^2 \frac{h_1^2}{d_1}.$$

Thus, we consider the new system of ODEs:

$$\begin{cases} \dot{h_1} = 8s^2 h_1 \log \left(-\frac{h_1}{2d_1} \right) - 4s^2 h_1; \\ \dot{d_1} = -s^2 \frac{h_1^2}{d_1}; \\ h_1(0) = h_{1,0}; \\ d_1(0) = d_{1,0}. \end{cases}$$
(3.29)

To find a solution to (3.29), we will analyze the behavior of

$$\frac{\mathrm{d}(h_1/d_1)}{\mathrm{d}T} = \frac{\dot{h_1}d_1 - \dot{d_1}h_1}{d_1^2}$$

By defining $y := h_1/d_1$, we obtain the following system in

$$\begin{cases} \dot{y} = s^2 y^3 + 4s^2 y \left(2\log\left(-\frac{y}{2} \right) - 1 \right) \\ y(0) = h_{1,0}/d_{1,0} = y_0. \end{cases}$$
 (3.30)

By imposing $\dot{y} = 0$, we find out that y = -2 for every T > 0 is a solution to (3.30). Since $y = h_1/d_1$, it follows that $h_1 = -2d_1$ is a solution to (3.29), so that

$$h_1(T) = 2d_{1,0} \exp(-4s^2T)$$
 and $d_1(T) = -d_{1,0} \exp(-4s^2T)$. (3.31)

As it can be observed, this solution holds only if $h_{1,0} = -2d_{1,0}$. This corresponds to studying the problem in a neighborhood where one of the defects is on the boundary and the other is not.

We compare, now, the behavior of the solution in (3.31) with the result obtained in (3.17) by studying the problem of an isolated disclination. From an analytical perspective, we can observe that:

$$\rho(T) = \left(1 + \mu_0 \exp(-4s^2T)\right)^{-1/2} \approx 1 - \mu_0 \frac{\exp(-4s^2T)}{2} \approx 1 - C \exp(-4s^2T);$$

$$d - \frac{h}{2} = \left(1 - \kappa d_{10} \exp(-4s^2T)\right) - \kappa d_{10} \exp(-4s^2T) = 1 - \kappa d_{10} \exp(-4s^2T)$$

$$\approx 1 - C \exp(-4s^2T).$$

The resulting error in norm L^{∞} is shown in Figure 3.9, using $\kappa = 10^{-\alpha}$, with $\alpha \in \{1, \ldots, 16\}$.

3.3.3 Region 2: convergent behavior

Within Region 2, we have $\dot{h} < 0$ and $\dot{d} < 0$, which means that we expect the dipole to collapse and its center to move toward the center of the disk. Referring to Figure 3.6, we study the case with green squares and the red boundary. It follows that within this region we have

$$0 < h(T) \le h_0 \le 1$$
 and $0 \le d(T) \le d_0 < \frac{1}{2}$, for all $T > 0$

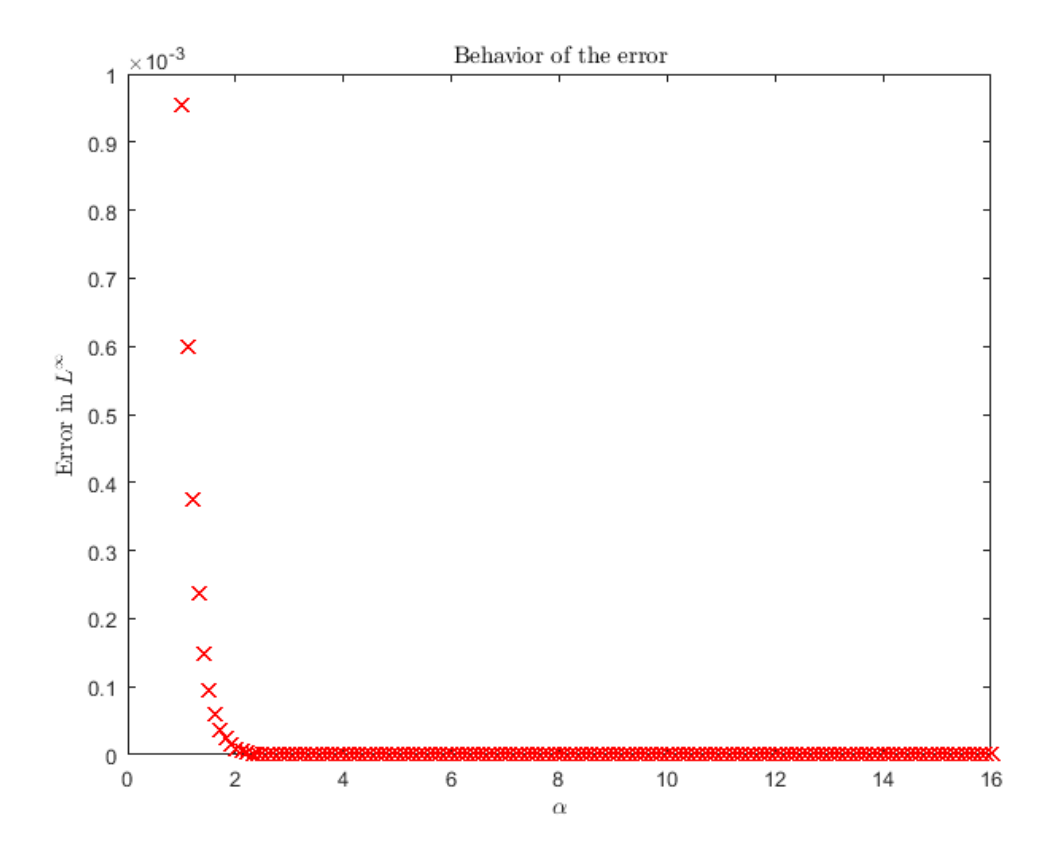


Figure 3.9: Behavior of the L^{∞} -error as $\kappa \to 0$.

In particular, we can define Region 2 as

$$\Omega_2 := \left\{ (h, d) \in (0, 1] \times [0, \frac{1}{2}] : d > \frac{h}{2} \quad \text{and} \quad f_1 < -f_2 \right\} \cap \tilde{\Omega}.$$
(3.32)

From Lemma 3.3.1, we know that $h \to 0$ and $d \to \bar{d}$, where $\bar{d} \in [0, d_0)$. In the same fashion as in the analysis of Region 1, we would like to characterize these behaviors.

Theorem 3.3.2 (Bounds for f and g in Ω_2). Consider $(h, d) \in \Omega_2$, then there exist functions $h_l^{(2)}, h_u^{(2)} : \mathbb{R}^+ \to \mathbb{R}$ such that:

$$h_l^{(2)}(T) \le h(T) \le h_u^{(2)}(T)$$
, for every $T > 0$

with $h_l^{(2)}$ defined by

$$h_l^{(2)}(T) = C_{1l} \exp(-C_{2l} \exp(8s^2T)),$$

with
$$C_{1l} := \frac{h_0^2 + 4}{4}$$
 and $C_{2l} := \log(C_{1l}/h_0)$, while $h_u^{(2)}$ is defined by
$$h_u^{(2)}(T) = C_{1u} \exp(-C_{2u} \exp(8s^2T)),$$

where $C_{1u} := 1 - d_0^2$ and $C_{2u} := \log(C_{1u}/h_0)$. There exist functions $d_l^{(2)}, d_u^{(2)} : \mathbb{R}^+ \to \mathbb{R}$ such that:

$$d_l^{(2)}(T) \le d(T) \le d_u^{(2)}(T), \quad \text{for every } T > 0$$

where $d_l^{(2)}, d_u^{(2)}$ are defined by:

$$d_l^{(2)}: \qquad \frac{4}{h_0^2} \log \left(\frac{d}{d_0} \right) + \left(\frac{1}{2} - \frac{2}{h_0^2} \right) \log \left(\left| \frac{h_0^2 - 4d^2}{h_0^2 - 4d_0^2} \right| \right) = -4s^2 \int_0^T h^2(t) dt,$$

$$d_u^{(2)}: \qquad \frac{h_0^2 + 4}{4} \left(\frac{1}{d^2} - \frac{1}{d_0^2} \right) + 2\log \left(\frac{d}{d_0} \right) = -4s^2 \int_0^T h^2(t) dt.$$

Proof. As in the proof of Theorem 3.3.2, we consider $\dot{h} = f_1(h, d) + f_2(h, d)$ and we notice that $f_2 \sim o(h)$ for all d, as $h \to 0$, so we neglect it. We now estimate f_1 as follows:

$$0 \le h \le h_0,$$

$$0 \le d \le d_0,$$

$$4(1 - d_0^2) \le h_0^2 + 4 - 4d^2 \le h_0^2 + 4,$$

$$\frac{1}{h_0^2 + 4} \le \frac{1}{h^2 + 4 - 4d^2} \le \frac{1}{4(1 - d_0^2)},$$

$$\frac{4h}{h_0^2 + 4} \le \frac{4h}{h^2 + 4 - 4d^2} \le \frac{h}{1 - d_0^2},$$

$$\log\left(\frac{4h}{h_0^2 + 4}\right) \le \log\left(\frac{4h}{h^2 + 4 - 4d^2}\right) \le \log\left(\frac{h}{1 - d_0^2}\right),$$

$$8s^2h \log\left(\frac{4h}{h_0^2 + 4}\right) \le 8s^2h \log\left(\frac{4h}{h^2 + 4 - 4d^2}\right) \le 8s^2h \log\left(\frac{h}{1 - d_0^2}\right).$$

$$(3.33)$$

Notice that $8s^2h\log\left(\frac{h}{1-d_0^2}\right) < 0 \text{ if } h < 1 - d_0^2.$

From Lemma 3.3.2 it follows that exist $h_l^{(2)}, h_u^{(2)} : \mathbb{R}^+ \to \mathbb{R}$ such that:

• $h_l^{(2)}$ is the solution to the problem $\dot{h} = 8s^2h\log\left(\frac{4h}{h_0^2+4}\right)$, which is

$$h_l^{(2)}(T) := \frac{h_0^2 + 4}{4} \exp\left(-\log\left(\frac{h_0^2 + 4}{4h_0}\right) \exp(8s^2T)\right);$$
41

• $h_u^{(2)}$ is the solution to the problem $\dot{h} = 8s^2h\log\left(\frac{h}{1-d_0^2}\right)$, which is

$$h_u^{(2)}(T) = (1 - d_0^2) \exp\left(-\log\left(\frac{h_0}{1 - d_0^2}\right) \exp(8s^2T)\right).$$

Regarding the forcing term for \dot{d} , we can highlight the following features:

$$\frac{-4d^2}{h_0^2 + 4 - 4d^2} \le \frac{h^2 - 4d^2}{h^2 + 4 - 4d^2} \le \frac{h_0^2 - 4d^2}{4(1 - d^2)},$$

$$\frac{-8h^2d^3}{h_0^2 + 4 - 4d^2} \le 2h^2 \frac{h^2 - 4d^2}{h^2 + 4 - 4d^2} d \le \frac{h^2}{2} \frac{h_0^2 - 4d^2}{1 - d^2} d,$$

$$-s^2 \frac{h^2}{2} \frac{h_0^2 - 4d^2}{1 - d^2} d \le -2s^2 h^2 \frac{h^2 - 4d^2}{h^2 + 4 - 4d^2} d \le s^2 \frac{+8h^2d^3}{h_0^2 + 4 - 4d^2}.$$
(3.34)

From Lemma 3.3.2 it follows that exist $d_l^{(2)}, d_u^{(2)}: \mathbb{R}^+ \to \mathbb{R}$ such that

$$d_l^{(2)}: \qquad \frac{4}{h_0^2} \log \left(\frac{d}{d_0} \right) + \left(\frac{1}{2} - \frac{2}{h_0^2} \right) \log \left(\left| \frac{h_0^2 - 4d^2}{h_0^2 - 4d_0^2} \right| \right) = -4s^2 \int_0^T h^2(t) \, dt,$$

$$d_u^{(2)}: \qquad \frac{h_0^2 + 4}{4} \left(\frac{1}{d^2} - \frac{1}{d_0^2} \right) + 2\log \left(\frac{d}{d_0} \right) = -4s^2 \int_0^T h^2(t) \, dt.$$

Corollary 3.3.3 (Regularity of h in Ω_2). In Ω_2 , we state that $h \in L^2(\mathbb{R}^+)$.

Proof. From the definition of $h_l^{(2)}$ and $h_u^{(2)}$ obtained from Theorem 3.3.2, we can conclude by computation (similar to that of Corollary 3.3.1) that $h_l^{(2)}, h_u^{(2)} \in L^2(\mathbb{R}^+)$.

Proposition 3.3.3 (Collision time in Ω_2). In Ω_2 , the defect collision occurs at infinite times.

Proof. From Lemma 3.3.1, we know that $h \to 0$ in Ω_2 , so it is sufficient to use the estimate of the lower bound to draw conclusions. From Theorem 3.3.2 we know that $h_l^{(2)}$ is a lower bound for h and we observe that $h_l^{(2)} \to 0$ as $T \to +\infty$. So, by comparison we can conclude that $h \to 0$ as $T \to +\infty$, which means that the collision occurs at infinite times.

Remark 3.3.3. We can observe that, when $h_0 \ll 1$, the estimates in (3.33) reduces to:

$$8s^2h\log(h) \le \dot{h} \le 8s^2h\log\left(\frac{h}{1-d_0^2}\right).$$

When we consider $d_0 = 0$, meaning the case of a disclination dipole symmetric to the origin of the disk with a fixed center of the dipole, we obtain

$$\dot{h} = 8s^2 h \log(h),$$

thus recovering the estimate in [11, Section 4.3].

3.3.4 Region 3: diverging behavior

In Region 3, we have $\dot{h} > 0$ and $\dot{d} < 0$, which means we expect the dipole to diverge and the center to move towards the boundary. Referring to Figure 3.6, we study the case with the blue squares and the red boundary. It follows that within this Region, we have

$$0 < h_0 \le h(T) < 2$$
 $0 \le d(T) \le d_0 \le \frac{1}{2}$, for all $T > 0$.

In particular, we define Region 3 as

$$\Omega_3 := \{(h,d) \in (0,2) \times [0,\frac{1}{2}] : f_1 > -f_2\} \cap \tilde{\Omega}$$

From Lemma 3.3.1, we know that in this region $h \to 2$ and $d \to 0$. We are interested in understanding how $h \to 2$, particularly in estimating the rate at which it happens.

Theorem 3.3.3 (Bounds for f in Ω_3). Consider $(h,d) \in \Omega_3$, then there exists $h_u^{(3)} : \mathbb{R}^+ \to \mathbb{R}$ such that

$$0 \le h(T) \le h_u^{(3)}(T), \quad \text{for all } T > 0.$$

where $h_u^{(3)}$ is defined as the solution to

$$\dot{h} = s^2 h \frac{4 - h^2 + 8d_0^4}{2 - d_0^2}. (3.35)$$

Proof. As in the proof of Theorem 3.3.1, we consider $\dot{h} = f_1 + f_2$. In Ω_3 , we observe that $f_1 \leq 0$, while $f_2 \geq 0$. Now, we focus on (f_2) :

$$\begin{split} h^2 - 8d_0^4 - 4 &\leq 2h^2d^2 + h^2 - 8d^4 + 12d^2 - 4 \leq 0 \\ \frac{h}{2 - d_0^2} (h^2 - 8d_0^4 - 4) &\leq \frac{4h}{h^2 + 4 - 4d^2} (2h^2d^2 + h^2 - 8d^4 + 12d^2 - 4) \leq 0 \\ 0 &\leq -4h \frac{2h^2d^2 + h^2 - 8d^4 + 12d^2 - 4}{h^2 + 4 - 4d^2} &\leq \frac{h}{2 - d_0^2} (4 - h^2 + 8d_0^4) \\ 0 &\leq \dot{h} \leq s^2 \frac{h}{2 - d_0^2} (4 - h^2 + 8d_0^4) \end{split}$$

From Lemma 3.3.2 it follows that exist $h_u^{(3)}: \mathbb{R}^+ \to \mathbb{R}$ such that $h_u^{(3)}$ is the solution to the problem

$$\dot{h} = s^2 \frac{h}{2 - d_0^2} (4 - h^2 + 8d_0^4).$$

In particular, $h_u^{(3)}$ is defined as follows:

$$h(T)^{2}(4-h(T)^{2}+8d_{0}^{4})^{2}=h_{0}(4+8d_{0}^{4}-h_{0}^{2})^{2}\exp\left(4s^{2}\frac{1+2d_{0}^{4}}{2-d_{0}^{2}}T+C\right),$$

where C is a constant to be determinated by imposing the initial condition. \Box

Limit case

Observe that in (3.35) for $d_0 = 0$, we recover the behavior of the symmetric dipole of disclinations as defined in [11]:

$$\dot{h} = s^2 h \frac{4 - h^2 + 8d_0^4}{2 - d_0^2} \sim 2s^2 h \left(1 - \left(\frac{h}{2} \right)^2 \right)$$
 (3.36)

What we want to highlight is that this behavior is effectively reducible to that of an isolated disclination: the defects are sufficiently far apart to not experience mutual attraction, and they tend towards the boundary as if they were the only defects in the domain, as proved in the following proposition.

Proposition 3.3.4 (Behavior of diverging dipole). In Ω_3 , the defects behave as if they were isolated defects.

Proof. For the sake of clarity, we recall the definition of the problem of an isolated disclination introduced in (3.17) and the problem of a diverging dipole (3.36) in the limit of $d \to 0$ and $h \to 2$.

$$\begin{cases} \dot{\rho} = 2s^2(1 - \rho^2)\rho \\ \dot{h} = 4s^2(2 - h) \\ h \to 2, d \to 0, \end{cases}$$
 (3.37)

where ρ represents the distance between the position of the defect and the center of the domain, and h represents the distance between the two defects symmetrically placed relative to the center of the domain.

Considering the first equation and multiplying both sides by 2ρ , we can rewrite the equation as:

$$\hat{\rho}^2 = 4s^2(1-\rho^2)\rho^2.$$

Considering the asymptotic behavior in the limit of $\rho \to 1$, we obtain the following equation:

$$\dot{\hat{\rho}^2} = 4s^2(1 - \rho^2).$$

By imposing $\rho^2 = h/2$, we can define the equivalence between the two behaviors in the limit.

3.4 Anisotropic scenario

Now, let us return to (3.10) and consider an anisotropic scenario for the dynamics of a disclination dipole. It is possible to perform a nondimensionalization of the problem by introducing the following scaled variables:

$$Y_k = \frac{y^k}{R}$$
 $X = \frac{x}{R}$, $\mathcal{G} = CH$, $T = \frac{\lambda C}{R^2}t$,

where

$$C = \frac{ER^2}{16\pi(1-\nu^2)}$$
 and $\lambda = 1 \,\mathrm{s\cdot kg}^{-1}$.

Let us introduce $\lambda_1 := \lambda_1(Y_1, Y_2)$ and $\lambda_2 := \lambda_2(Y_1, Y_2)$, to be determinated later, so that:

$$\begin{cases} \dot{Y}_1 = -\lambda_1 \nabla_{Y_1} H(Y_1, Y_2); \\ \dot{Y}_2 = -\lambda_2 \nabla_{Y_2} H(Y_1, Y_2). \end{cases}$$
(3.38)

We can proceed as in the isotropic scenario, by introducing

$$F_1 := -\nabla_{Y_1} H$$
 and $F_2 := -\nabla_{Y_2} H$,

and the change of variables

$$Y_1 = d + \frac{h}{2}$$
 and $Y_2 = d - \frac{h}{2}$.

At this point, we can derive the dynamics of h distance between the defects and d center of the dipole. The problem now reads

$$\begin{cases} \dot{h} = \lambda_1 F_1 - \lambda_2 F_2, \\ \dot{d} = (\lambda_1 F_1 + \lambda_2 F_2)/2. \end{cases}$$

We define $k, p \in \mathbb{R}$ such that

$$\begin{cases} \lambda_1 F_1 + \lambda_2 F_2 = k(F_1 + F_2), \\ \lambda_1 F_1 - \lambda_2 F_2 = p(F_1 - F_2), \end{cases}$$
(3.39)

meaning that we are considering the case with

$$\begin{cases} \lambda_1 = \frac{k(F_1 + F_2) + p(F_1 - F_2)}{2F_1}, \\ \lambda_2 = \frac{k(F_1 + F_2) - p(F_1 - F_2)}{2F_2}. \end{cases}$$

In particular, we are interested in analyzing two scenarios:

- (k, p) = (1,0), which corresponds to a dipole with a fixed distance between the defects and a movable center;
- (k, p) = (0,1), which corresponds to a dipole with a fixed center and a movable distance between the defects.

3.4.1 Fixed distance behavior

We consider λ_1, λ_2 so that (k, p) = (1,0) and the following resulting system

$$\begin{cases}
\dot{h} = 0; \\
h(0) = h_0;
\end{cases}
\begin{cases}
\dot{d} = -2s^2 h_0^2 d \frac{h_0^2 - 4d^2}{h_0^2 - 4d^2 + 4}; \\
d(0) = d_0.
\end{cases}$$
(3.40)

The problem now reads

$$\begin{cases} \dot{d} = -2s^2 h_0^2 d \frac{h_0^2 - 4d^2}{h_0^2 - 4d^2 + 4} =: \bar{g}(d) \\ d(0) = d_0 \end{cases}$$
 (3.41)

and we observe that

$$\begin{cases} \dot{d} < 0 & \text{if } d < h_0/2, \\ \dot{d} > 0 & \text{if } d > h_0/2. \end{cases}$$

We are considering the problem where the distance h is held constant at h_0 and the center of the dipole evolves over time. This simplification allows us to focus on the dynamics of the dipole center, without the added complexity of the changing distance, thus reducing the problem to one involving only the movement of the center of the dipole.

Lemma 3.4.1 (Stationary points). Consider (k, p) = (1,0). Fixing $h_0 \in (0,2)$, it follows that

- d = 0 is a stable stationary point when $\dot{d} < 0$;
- $d = h_0/2$ is an unstable stationary point.

Proof. By the computation of

$$J_d(d) := \bar{g}'(d) = \frac{-2s^2 h_0^2}{h_0^2 - 4d^2 + 4} \left(h_0^2 - 4d^2 - \frac{32d^2}{h_0^2 - 4d^2 + 4} \right),$$

we observe that:

• $J_d(d=0) = -\frac{2s^2 h_0^4}{h^2+4} < 0$, so d=0 is a stable point when $\dot{d} < 0$;

•
$$J_d(d = h_0/2) = s^2 h_0^4 > 0$$
, so $d = h_0/2$ is an unstable point.

Remark 3.4.1. The solution to system (3.41) is the following implicit solution

$$\log\left(\frac{d}{d_0}\right) - \frac{2}{h_0^2}\log\left(\frac{d_0^2}{d^2}\left|\frac{h_0^2 - 4d^2}{h_0^2 - 4d_0^2}\right|\right) + 2s^2h_0^2T = 0.$$
(3.42)

In Figure 3.10 we represent the numerical solution at $h_0 \in [2d_0, 2-2d_0]$ fixed, in particular in Figure 3.10a we present the $\dot{d} > 0$ scenario, while in Figure 3.10b the $\dot{d} < 0$ scenario. As it can be observed, in the first case, $d \to 1$ in a finite time, whereas in the second case, the numerical simulations suggests that $d \to 0$ in an infinite time; we make this intuition formal in the following proposition.

Proposition 3.4.1 (Collision with the boundary). In the fixed distance scenario, the center of the dipole d reaches the boundary in finite time \bar{T} when $\dot{d} > 0$, while it reaches the center of the unit disk for infinite time when $\dot{d} < 0$.

Proof. From (3.42) we can compute the time T as:

$$T = \frac{1}{2s^2h_0^2} \left(\log \frac{d_0}{d} + \frac{2}{h_0^2} \log \left(\frac{d_0^2}{d^2} \left| \frac{h_0^2 - 4d}{h_0^2 - 4d_0^2} \right| \right) \right). \tag{3.43}$$

Now, if we suppose that d reaches the boundary, meaning that d = 1, we can find that the time \bar{T} needed is

$$\bar{T} := \frac{1}{2s^2h_0^2}\log d_0 + \frac{1}{s^2h_0^4}\log\left(d_0^2\left|\frac{h_0^2 - 4}{h_0^2 - 4d_0^2}\right|\right).$$

Similarly, if we suppose that $d \to 0$, meaning that the center of the dipole approaches the center of the disk, we find that $\tilde{T} \to +\infty$, which is the time required in this case.

3.4.2 Fixed center of the dipole

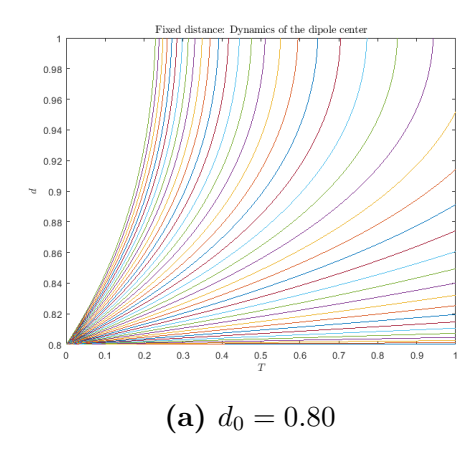
By imposing λ_1, λ_2 so that (k, p) = (0,1) in (3.39), it follows that

$$\begin{cases} \dot{d} = 0, \\ d(0) = d_0, \end{cases}$$
 (3.44)

and the problem for h now reads

$$\begin{cases}
\dot{h} = 8s^2 h \log\left(\frac{4h}{h^2 + 4 - 4d_0^2}\right) - 4s^2 h \frac{h^2 (2d_0^2 + 1) - 8d_0^4 + 12d_0^2 - 4}{h^2 + 4 - 4d_0^2} =: \bar{f}(h), \\
h(0) = h_0,
\end{cases} (3.45)$$

representing the fixed center of the dipole, $d(T) = d_0$ for every T > 0, and a moving distance between the two defects.



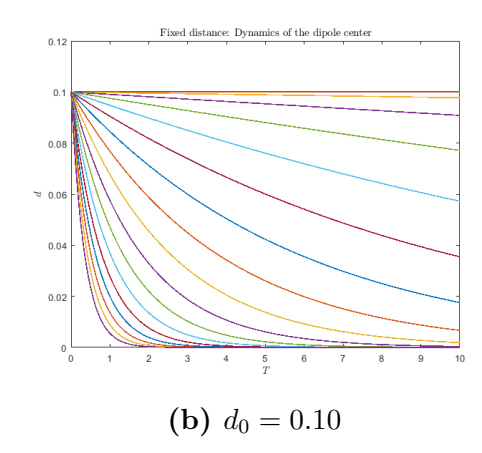


Figure 3.10: Behavior of a dipole of disclinations with a fixed distance, varying h_0 from bottom $h_0 = 0.01$ to top $h_0 = 2 - 2d_0$, with $d_0 = 0.80$ (left) and $d_0 = 0.10$ (right).

Lemma 3.4.2 (Stationary points). Consider (k, p) = (0,1). Fixing $d_0 \in [0,1)$, it follows that

- h = 2 is an asymptotically stable point;
- h^* such that $\log\left(\frac{4h}{h^2+4-4d_0^2}\right) \frac{h^2(2d_0^2+1)-8d_0^4+12d_0^2-4}{h^2+4-4d_0^2} = 0$ is an unstable stationary point;
- h = 0, for every $d_0 \in [0,1)$, is an asymptotically stable point.

Proof. By the computation of

$$J_h(h) := \bar{f}'(h)$$

$$= 8s^2 \left[\log(\frac{4h}{h^2 + 4 - 4d_0^2}) + \frac{4 - 4d_0^2 - h^2}{h^2 + 4 - 4d_0^2} - 4\frac{h^4(2d_0^2 + 2) + (8 - 8d_0^2 - h^2)}{(h^2 + 4 - 4d_0^2)^2} \right],$$
(3.46)

we observe that:

- $J_h(2) = 16s^2 \log \left(-\frac{2}{d_0^2-2}\right) s^2 \frac{8d_0^2 \left(2d_0^2-5\right)}{d_0^2-2} < 0$, so h=2 is an asymptotically stable point when d_0, h so that $\dot{h} > 0$;
- $J_h(h^*) > 0$, where h^* is the solution to $\log\left(\frac{4h}{h^2+4-4d_0^2}\right) \frac{h^2(2d_0^2+1)-8d_0^4+12d_0^2-4}{h^2+4-4d_0^2} = 0$, is an unstable point.

To prove that h=0 is an asymptotically stable point when $\dot{h}<0$ we refer to the proof of Lemma 3.3.1.

Proposition 3.4.2 (Bounds for f). In the region in which $\dot{h} \leq 0$ is true that:

$$h_l \leq h \leq h_u$$

with h_l solution to $\dot{h} = 8s^2h \log(\frac{4h}{h_0^2+4-4d_0^2})$, while h_u solution to $\dot{h} = 8s^2h \log(\frac{h}{1-d_0^2})$. In the region in which $\dot{h} > 0$ is true that

$$h < h_u$$
.

with h_u solution to $\dot{h} = -4s^2h \frac{h^2(2d_0^2+1)-8d_0^2+12d_0^2-4}{h_0^2+4-4d_0^2}$.

Proof. First, let us consider

$$f(h,d) = \underbrace{8s^2h\log\left(\frac{4h}{h^2 + 4 - 4d_0^2}\right)}_{f_1(h)} + \underbrace{\frac{-4s^2h}{h^2 + 4 - 4d_0^2}(2h^2d_0^2 + h^2 - 8d_0^4 + 12d_0^2 - 4)}_{f_2(h)}$$

In the region in which $\dot{h} \leq 0$, we know that $h \to 0$, so $f_2 \sim o(h)$ and we neglect it. We can estimate f_1 as follow:

$$\begin{aligned} 4(1-d_0^2) & \leq h^2 + 4 - 4d_0^2 \leq h_0^2 + 4 - 4d_0^2 \\ \frac{1}{h_0^2 + 4 - 4d_0^2} & \leq \frac{1}{h^2 + 4 - 4d_0^2} \leq \frac{1}{4(1 - d_0^2)} \\ 8s^2 h \log \left(\frac{4h}{h_0^2 + 4 - 4d_0^2} \right) & \leq 8s^2 h \log \left(\frac{4h}{h^2 + 4 - 4d_0^2} \right) \leq 8s^2 h \log \left(\frac{h}{1 - d_0^2} \right) \end{aligned}$$

We can now apply Lemma 3.3.2 and conclude that exist $h_l, h_u : \mathbb{R}^+ \to \mathbb{R}$ so that

$$h_l \leq h \leq h_u$$
.

In particular,

1.

$$h_l(T) = C_{1l} \exp(-C_{2l} \exp(8s^2T))$$

is the solution to the problem $\dot{h} = 8h \log \left(\frac{4h}{h_0^2 + 4 - 4d_0^2}\right)$, with $C_{1l} = \frac{h_0^2 + 4 - 4d_0^2}{4}$ and $C_{2l} = \log(C_{1l}/h_0)$;

2.

$$h_u(T) = C_{1u} \exp(-C_{2u} \exp(8s^2T))$$

is the solution to the problem $\dot{h} = 8h \log \left(\frac{h}{1-d_0^2}\right)$, with $C_{1u} = 1 - d_0^2$ and $C_{2u} = \log(C_{1u}/h_0)$.

In the region in which $\dot{h} > 0$, $f_1 \le 0$ and $f_2 \ge 0$, so we can estimate f_2 as follow:

$$0 \leq -4s^2h\frac{h^2(2d_0^2+1)-8d_0^2+12d_0^2-4}{h^2+4-4d_0^2} \leq -4s^2h\frac{h^2(2d_0^2+1)-8d_0^2+12d_0^2-4}{h_0^2+4-4d_0^2}.$$

Applying Lemma 3.3.2, then exists $h_u: \mathbb{R}^+ \to \mathbb{R}$ so that

$$h \leq h_u$$
.

In particular,

$$h_u(T) = \sqrt{\frac{C_{1u} \exp(-8s^2T)}{1 - C_{2u} \exp(-8s^2T)}},$$

with $C_{1u} := \frac{D}{k} \exp(\frac{D}{h_0^2 + 4 - 4d_0^2})$, $C_{2u} := \frac{C}{k} \exp(\frac{D}{h_0^+ 4 - 4d_0^2})$, $C = 2d_0^2 + 1$, $D = 12d_0^2 - 4 - 8d_0^4$ and $k = \frac{Ch_0^2 + D}{h_0^2}$, is the solution to

$$\dot{h} = -4s^2 h \frac{h^2 (2d_0^2 + 1) - 8d_0^2 + 12d_0^2 - 4}{h_0^2 + 4 - 4d_0^2}.$$
 (3.47)

Corollary 3.4.1 (Properties of h). In the fixed center of the dipole, it holds that:

- 1. $h \in L^2$, when $\dot{h} < 0$;
- 2. $h \to 0$ as $T \to +\infty$, when $\dot{h} < 0$;
- 3. when $h \to 2$ and $d_0 \to 0$, each defect behaves like an isolated defect.

Proof. In the same fashion of Propositions 3.3.1 and 3.3.3, we can use the results of Proposition 3.4.2 to observe that $h_l, h_u \in L^2(\mathbb{R}^+)$ and so by comparison it follows that $h \in L^2(\mathbb{R}^+)$. We also observe that $h_l, h_u \to 0$ as $T \to +\infty$, so it follows that $h \to 0$ as $T \to +\infty$.

From (3.47), considering $d \to 0, h \to 2^-$ we obtain

$$\dot{h} = 2s^2 \left(1 - \left(\frac{h}{2}\right)^2\right),\,$$

recovering the same dynamical system presented in Proposition 3.3.4.

Remark 3.4.2. When $h_0 \ll 1$, then

$$\dot{h} = 8s^2 h \log \left(\frac{h}{1 - d_0^2}\right),$$

whose solution is

$$h(T) = (1 - d_0^2) \exp\left(-\log\left(\frac{1 - d_0^2}{h_0}\right) \exp(8s^2T)\right).$$

Remark 3.4.3. When $d_0 = 0$, meaning we are considering the case with symmetric disposition of defects with respect to the center of the disk, we find the case analyzed in [11].

Chapter 4

Edge dislocation

The purpose of this section is to derive the formulation of the dynamics of an edge dislocation by establishing its energetic equivalence with the rescaled energy of a colliding dipole of disclinations [10]. In this framework, the energetic formulation of a dislocation is expected to yield a diverging minimal energy in the limit $h \to 0$. In fact, it is known that the energy related to dislocations is diverging near the singularity (see, e.g., [9, 27, 29, 43]). Cermelli and Leoni, in [8], introduce a variational technique known as the *core-radius regularization approach*, which rigorously establishes the possibility of focusing solely on the regular part of the energy to fully describe all the information regarding self and mutual interactions between dislocations. As discussed in Chapter 2, this technique allows one to consider the domain excluding a core of radius $\varepsilon > 0$ around the singularity, and to expand the minimum energy as $\varepsilon \to 0$. Following this expansion, the minimum energy can be expressed as:

$$\mathcal{H}(x;\Omega) = \frac{E}{1-\nu^2} \frac{|b|^2}{8\pi} |\log \varepsilon| + \mathcal{H}_{ren}(x) + o(\varepsilon), \tag{4.1}$$

where the first term is diverging as $\varepsilon \to 0$, and b denotes the Burgers vector associated with a dislocation sitting at x; the term \mathcal{H}_{ren} represents the regular part of the asymptotic expansion, commonly referred to as the renormalized energy; the remainder term $o(\varepsilon)$, as $\varepsilon \to 0$, accounts for the negligible contributions to the energy. As shown in [8], the dislocation problem can be fully characterized by focusing solely on the renormalized energy \mathcal{H}_{ren} .

In a similar spirit, we propose a core-radius type approach to extract, from the rescaled energy of a collapsing dipole of disclinations, the formulation of the minimum energy associated with an edge dislocation sitting at the center of the dipole. This dislocation has a Burgers vector b rotated by $\pi/2$ with respect to the axis of the dipole, denoted by e. It is important to note that, in contrast to the core-radius regularization approach in [8], we propose a regularization in the

limit as h, the distance between the two disclinations, tends to zero. Once the energy of an edge dislocation is obtained, we proceed as in Chapter 3 and [11] for disclinations, and as in [1, 4, 5, 8, 29] for screw dislocations: we assume that the dynamics of edge dislocations can be derived via the maximal dissipation criterion. Finally, we analyze the dynamics of a single edge dislocation in the unit disk.

4.1 The energy of an edge dislocation

The idea is to follow the argument in [10, Section 4], in order to show the energetic equivalence between a dipole of disclinations and an edge dislocation. We consider the rescaled energy functional introduced in (2.24):

$$\mathcal{J}^h(w;\Omega) = \frac{1}{2} \frac{1+\nu}{E} \int_{\Omega} \left(|\nabla^2 w|^2 - \nu (\Delta w)^2 \right) \mathrm{d}x + \frac{s}{h} \left[w \left(x + \frac{h}{2} e \right) - w \left(x - \frac{h}{2} e \right) \right],$$

and we are interested in the minimization problem

$$\bar{w} = \arg\min \left\{ \mathcal{J}^h(w; \Omega) \,\middle|\, w \in H_0^2(\Omega) \right\}.$$

It can be shown, in the same way as for the disclination problem, that $H_0^2(\Omega)$ is the minimal regularity required to ensure the well-posedness of the problem for dislocations. By applying Clapeyron's theorem, one obtains the identity

$$\mathcal{G}(\bar{w},\Omega) = -\frac{1}{2}s\frac{\bar{w}(x+\frac{h}{2}e) - \bar{w}(x-\frac{h}{2}e)}{h}.$$
(4.2)

The variational problem associated with \mathcal{J}^h reads

$$\begin{cases}
\frac{1-\nu^2}{E}\Delta^2 w = -\frac{s}{h}(\delta_{x+h/2e} - \delta_{x-h/2e}) & \text{in } \Omega, \\
w = \partial_n w = 0 & \text{on } \partial\Omega,
\end{cases}$$
(4.3)

which can be reduced to the clamped disk problem [45], as in Chapter 3 and [11].

Thanks to the linearity of the biharmonic operator and the boundary conditions, the solution of the problem can be expressed as

$$\bar{w}(x) = \sum_{k=1}^{2} \bar{w}_k(x), \quad \text{with } \bar{w}_k(x) \coloneqq \begin{cases} \bar{p}_k(x), & x \in \Omega \setminus \{y^k\} \\ \bar{q}_k, & x = y^k, \end{cases}$$
(4.4)

where the functions $\bar{p}_k(x)$ and \bar{q}_k are explicitly given by:

$$\bar{p}_k(x) = -\frac{Cs_k}{h} \left[\frac{|x - y^k|^2}{R^2} \log \left(\frac{|x - y^k|^2}{R^2} \right) + \left(1 - \frac{|x|^2}{R^2} \right) \left(1 - \frac{|y^k|^2}{R^2} \right) - \frac{|x - y^k|^2}{R^2} \log \left(\frac{R^4 - 2R^2x \cdot y^k + |x|^2|y^k|^2}{R^4} \right) \right],$$

$$\bar{q}_k := -\frac{Cs_k}{h} \left(1 - \frac{|y^k|^2}{R^2} \right)^2,$$

where the constant C is defined in (3.9).

Substituting the expression for \bar{w} in (4.4) into the energy in (4.2), it follows that

$$\mathcal{G}(\bar{w}; B_R(0)) = -\frac{1}{2h} \sum_{k=1}^2 s_k \bar{w}(y^k) = -\frac{1}{2h} \sum_{k=1}^2 \sum_{\ell=1}^2 s_k \bar{w}_\ell(y^k) =$$

$$= -\frac{1}{2h} \sum_{k=1}^2 s_k \bar{w}_k(y^k) - \frac{1}{h} \sum_{k=1}^2 \sum_{\ell=k+1}^2 s_k \bar{w}_\ell(y^k) =$$

$$= -s \frac{\bar{q}_1 - \bar{q}_2}{2h} - s \frac{\bar{p}_2(y^1)}{h}$$

$$= -\frac{Cs^2}{2h^2} \left[\left(1 - \frac{|y^1|^2}{R^2} \right)^2 + \left(1 - \frac{|y^2|^2}{R^2} \right)^2 \right]$$

$$- \frac{Cs^2}{h^2} \left[\frac{|y^1 - y^2|^2}{R^2} \log \left(\frac{|y^1 - y^2|^2}{R^2} \right) + \left(1 - \frac{|y^1|^2}{R^2} \right) \left(1 - \frac{|y^2|^2}{R^2} \right) \right]$$

$$- \frac{|y^1 - y^2|^2}{R^2} \log \left(\frac{R^4 - 2R^2y^1 \cdot y^2 + |y^1|^2 |y^2|^2}{R^4} \right) \right].$$

We introduce a nondimensionalization of the problem by setting

$$Y_k = \frac{y^k}{R}, \qquad X = \frac{x}{R}, \qquad \mathcal{G} = CH, \qquad T = \frac{C}{R^2}t,$$

where C is defined in (3.9).

This leads to the expression

$$H(Y_{1}, Y_{2}) := -\frac{s^{2}}{2h^{2}} \left[(1 - |Y_{1}|^{2})^{2} + (1 - |Y_{2}|^{2})^{2} + 2|Y_{1} - Y_{2}|^{2} \log|Y_{1} - Y_{2}|^{2} \right]$$

$$+ 2(1 - |Y_{1}|^{2})(1 - |Y_{2}|^{2}) - 2|Y_{1} - Y_{2}|^{2} \log(1 - 2Y_{1}Y_{2} + |Y_{1}|^{2}|Y_{2}|^{2}) \right]$$

$$= -\frac{s^{2}}{2} \left[\frac{(1 - |Y_{1}|^{2})^{2}}{|Y_{1} - Y_{2}|^{2}} + \frac{(1 - |Y_{2}|^{2})^{2}}{|Y_{1} - Y_{2}|^{2}} + 2\log|Y_{1} - Y_{2}|^{2} \right]$$

$$+ 2\frac{(1 - |Y_{1}|^{2})(1 - |Y_{2}|^{2})}{|Y_{1} - Y_{2}|^{2}} - 2\log(1 - 2Y_{1} \cdot Y_{2} + |Y_{1}|^{2}|Y_{2}|^{2}) \right],$$

$$(4.5)$$

where we have used that $h = |Y_1 - Y_2|$. We now consider a radial dipole (see Section 3.3) and, without losing of generality, we assume that $Y_1 > Y_2$:

$$H(Y_1, Y_2) = s^2 \left[2 \log \left(\frac{1 - Y_1 Y_2}{Y_1 - Y_2} \right) + \frac{(Y_1 + Y_2)^2}{2} \right]. \tag{4.6}$$

To emphasize the contribution of the dipole, we substitute Y_1, Y_2 , the positions of the defects, into h, d, the distance between the defects and center of the dipole. The energy in (4.6) now reads

$$\hat{H}(h,d) := s^2 \left[2 \log \left(\frac{h^2 - 4 d^2 + 4}{4} \right) - \log \left(h^2 \right) + 2 d^2 \right]. \tag{4.7}$$

In particular, as $h \to 0$, the energy diverges. This behavior is expected, since the construction ultimately leads to the energy associated with an edge dislocation, which is known to diverge near the singularity. More specifically, from the formulation in (4.7) it follows that the only diverging contribution, in the limit $h \to 0$, is associated with the term $\log h^2$.

In the spirit of the core-radius approach, we isolate from the minimum energy \hat{H} the diverging contribution given by $\log h^2$

$$\hat{H}_{\text{ren}}(d) := \hat{H}(h, d) + s^2 \log(h^2) = 2s^2 \log\left(\frac{h^2 - 4d^2 + 4}{4}\right) + 2s^2 d^2.$$

By taking the limit as $h \to 0$, we obtain

$$\mathcal{W}(d) := \lim_{h \to 0} \hat{H}_{\text{ren}}(d) = \lim_{h \to 0} \left[2s^2 \log \left(\frac{h^2 - 4 d^2 + 4}{4} \right) + 2 s^2 d^2 \right]$$
$$= 2s^2 \left(\log(1 - d^2) + d^2 \right). \tag{4.8}$$

The formulation obtained in (4.8) represents the energy of an edge dislocation in a unit disk, which, after a $\pi/2$ -rotation (see (2.28)), can be expressed in terms of the magnitude of the Burgers vector b that characterizes the edge dislocation

$$W(d) := 2|b|^2 \left(\log(1 - d^2) + d^2\right). \tag{4.9}$$

4.2 Dynamics of an edge dislocation

The energy of an isolated edge dislocation in (4.9) already suggests a strong analogy with the energy of screw dislocations (see, e.g., [29, Formula (65)]) or with the dynamic contribution that emerges in the Cermelli–Leoni formulation of the Peach–Koehler force.

Assuming that the dynamics of edge dislocations, as with screw dislocations and disclinations, is governed by the maximal dissipation criterion, the evolution equation for d can be derived as the gradient flow of the energy:

$$\dot{d} = -\mathcal{W}'(d) = \frac{4|b|^2 d^3}{1 - d^2}. (4.10)$$

For the sake of consistency with the theory introduced in [10], we rename d, which originally represented the center of the disclination dipole, with x, which now represents the position of a dislocation. The resulting dynamics can therefore be formulated as

$$\begin{cases} \dot{x} = \frac{4|b|^2 x^3}{1 - x^2}, \\ x(0) = x_0. \end{cases}$$
 (4.11)

In particular, the implicit solution to this problem is given by

$$\log \frac{x^2}{x_0^2} + \frac{1}{x^2} - \frac{1}{x_0^2} + 8|b|^2 T = 0.$$
(4.12)

From this result, we can observe that $x^* = 0$ is an unstable equilibrium condition. This configuration corresponds to the solution where the dislocation remains stationary at the center of the disk $(x \equiv 0)$ due to the symmetry of the problem.

Proposition 4.2.1 (Collision time for an isolated edge dislocation). An isolated edge dislocation, initially positioned away from the origin $(d_0 \neq 0)$, reaches the boundary of the domain in the finite time

$$\bar{T} := \frac{1}{8|b|^2} \left(\log x_0^2 - 1 + \frac{1}{x_0^2} \right).$$
 (4.13)

Proof. Consider the problem formulated in (4.11) for a single edge dislocation in a unit disk, along with its solution in (4.12). By imposing that $x(\bar{T}) = 1$, which means that the dislocation has reached the boundary of the disk, we obtain:

$$-\log x_0^2 + 1 - \frac{1}{x_0^2} + 8|b|^2 \bar{T} = 0,$$

from which the collision time is derived as

$$\bar{T} := \frac{1}{8|b|^2} \left(\log x_0^2 - 1 + \frac{1}{x_0^2} \right).$$

Proposition 4.2.2 (Relation between an isolated edge dislocation and an isolated screw dislocation). By means of the maps

$$T \to \frac{t}{8|b|^2\pi}$$
 and $x^2(T) \mapsto \frac{1}{R(t)}$, (4.14)

a relationship between an isolated edge dislocation and an isolated screw dislocation can be established.

Proof. Consider the problem presented in [29, Section 4.2], where the dynamics of an isolated screw dislocation in a circular domain is discussed. Several similarities can be observed between this formulation and the edge dislocation case. Specifically, the paper provides an implicit formulation for the motion of a screw dislocation, given by

$$\log \frac{R(t)}{R_0} - R(t) + R_0 = \frac{t}{\pi}, \quad \text{for } t \in [0, \bar{t}_{coll}^{\partial \Omega}],$$
 (4.15)

where $R(t) := |z(t)|^2$ and $R_0 := |z(0)|^2$, with z(t) representing the position of the dislocation relative to the center of the domain and $\bar{t}_{coll}^{\partial\Omega}$ is the collision time defined in [29, Formula (67)] as

$$\bar{t}_{coll}^{\partial\Omega} := \pi((1 - \sqrt{R_0})^2 - 2(1 - \sqrt{R_0}) - \log R_0) = \pi(R_0 - 1 - \log R_0). \tag{4.16}$$

By comparing (4.12) and (4.15), (4.13) and (4.16), we observe a relationship between the two formulations. Specifically, by imposing the maps in (4.14), a direct connection between the dynamics of edge and screw dislocations can be established.

Theorem 4.2.1 (Convergence to an edge dislocation). By introducing the time rescaling

$$\tau(T) := \frac{1}{2} \int_0^T h^2(t) \, \mathrm{d}t,$$

in the dynamics of a converging disclination dipole (see (3.26) in Ω_1 and (3.34) in Ω_2), we can state that a converging disclination dipole is dynamically equivalent to an edge dislocation, see (4.11).

Proof. We begin by assuming the behavior of the disclination dipole in both regions Ω_1 (see Section 3.3.2) and Ω_2 (see Section 3.3.3). In Ω_1 , as $h_0 \ll 1$, the estimates introduced in (3.26) yield

$$\dot{d} = \frac{2s^2h^2d^3}{1 - d^2}. (4.17)$$

In the same fashion, in Ω_2 taking (3.34) into account, when $h_0 \ll 1$, we observe that

$$\dot{d} = \frac{2s^2h^2d^3}{1 - d^2}.$$

In both cases, the implicit solution of the problem is

$$\log\left(\frac{d^2}{d_0^2}\right) + \frac{1}{d^2} - \frac{1}{d_0^2} = -4s^2 \int_0^T h^2(t) dt.$$

In particular, by Propositions 3.3.1 and 3.3.3, $h \in L^2(\mathbb{R}^+)$ in $C \subseteq \Omega_1$ and in Ω_2 . We define

$$\tau(T) := \frac{1}{2} \int_0^T h^2(t) \, \mathrm{d}t, \tag{4.18}$$

and we note that $\tau(0) = 0$, the function τ is strictly increasing, and it converges to a finite limit as $T \to +\infty$

$$\tau_{\infty} := \lim_{T \to +\infty} \tau(T) = \frac{1}{2} \int_0^{\infty} h^2(t) dt.$$

Therefore, τ is a strictly increasing and positive function, so that we have:

$$0 < \tau(T) \le \tau_{\infty} < +\infty$$
, for every $T > 0$.

The introduction of this time rescaling allows us to suppress the transient contribution and observe the behavior of the center of the dipole over longer timescales, thereby highlighting the long-time dynamics of an edge dislocation.

In particular, the monotonicity of τ allows us to apply the Inverse Function Theorem, and thus conclude the existence of a bijective map $\sigma:[0,\tau_{\infty}]\to\mathbb{R}^+$ such that $\sigma(\tau)=T$. This, in turn, allows us to formally rewrite the problem in terms of the new variable τ . Specifically, we observe that:

$$d(T) = d(\sigma(\tau)) = \tilde{d}(\tau).$$

We now rewrite (4.17) in terms of \tilde{d} and τ :

$$\dot{\tilde{d}} = \frac{4s^2\tilde{d}^3}{1 - \tilde{d}^2},$$

whose implicit solution is given by:

$$\log\left(\frac{\tilde{d}^2}{\tilde{d_0}^2}\right) + \frac{1}{\tilde{d}^2} - \frac{1}{\tilde{d_0}^2} + 8s^2\tau = 0. \tag{4.19}$$

From this solution we can observe that the time $\bar{\tau}$ needed to reach the boundary $(\tilde{d}=1)$ is finite and can be computed as:

$$\bar{\tau} = \frac{1}{8s^2} \left(\log(\tilde{d_0}^2) - 1 + \frac{1}{\tilde{d_0}^2} \right).$$

The result obtained in (4.19) is the description of an edge dislocation, derived through a time rescaling from the collision of a dipole of disclinations.

Remark 4.2.1. It is worth noting that the assumption $h \in L^2$ is not strictly required in order to introduce the time rescaling. However, it plays a key role in ensuring that $\tau \in [0, \tau_{\infty}]$, with $\tau_{\infty} < +\infty$, thus reinforcing the analogy with the formulation for dislocations. Without this assumption, the integral defining τ could diverge, potentially preventing a complete identification between the two dynamics.

Remark 4.2.2. In a similar fashion, this result can also be extended to the case of the fixed-arm configuration (see Section 3.4.1).

Specifically, by dividing the system in (3.41) by $\frac{1}{2}h_0^2$, considering the limiting case as $h_0 \to 0$, and performing a suitable expansion, we obtain the following implicit formulation:

$$\frac{1}{d^2} - \frac{1}{d_0^2} + \log\left(\frac{d^2}{d_0^2}\right) + 8s^2T = 0.$$

This leads to the formulation of the dynamics of an edge dislocation in (4.12).

This result, which can be interpreted as an extension, from the dynamical point of view, of the Eshelby's equivalence, not only provides a consistent formulation for the motion of edge dislocations in the unit disk, but also reveals a deeper structural connection with the theory of the two defects.

We can therefore conclude that the dynamics of edge dislocations may be naturally obtained from the limit behavior of collapsing disclination dipoles. This observation also opens the door to the possibility of constructing explicit mappings between models describing edge and screw dislocations and disclinations.

Chapter 5

Conclusions and perspectives

In this thesis we have investigated the variational formulation of the elastic energy in the presence of crystalline defects, with particular attention to disclinations and their relation to dislocations. Starting from the classical framework of linearized elasticity, we have introduced incompatibilities to model the presence of topological defects. In particular, we have focused on disclinations, characterized by the Frank angles, and on their energetic and variational description.

A central starting point of this work is the rigorous derivation of the variational model for disclinations, and the subsequent analysis of its scaling limit, which shows the energetic equivalence with edge dislocations. This result is consistent with Eshelby's equivalence, and provides a solid mathematical framework for interpreting disclinations as *precursors* of dislocations in the appropriate limit. The rescaling argument and the limiting process not only highlight the structural analogies between the two types of defects, but also justify the passage from one model to the other within a unified variational perspective.

From a numerical standpoint, we observed that the problem is often affected by ill-conditioning, which makes the computation of solutions particularly challenging. A more systematic analysis of the numerical sources of instability would be desirable, possibly leading to the construction of efficient preconditioners or alternative discretization strategies. Such an investigation could open the way to more robust simulations, especially when extending the model to multiple interacting defects.

Future developments of this research may include the extension of the present model to a larger number of defects, both of the same type and of different types, in order to analyze their mutual interactions. From the analytical viewpoint, a careful study of regularity and convexity properties of the variational functional could further strengthen the mathematical foundation of the model. From the numerical viewpoint, it would be particularly relevant to explore the long-time behavior of defect dynamics: as shown by our analysis, disclinations tend to move toward the boundary as time tends to infinity, and their collision occurs only asymptotically.

To conclude, this thesis has confirmed the validity of the variational description of disclinations, its connection to the theory of dislocations, and its consistency with Eshelby's equivalence. The results obtained not only enrich the theoretical understanding of crystalline defects, but also suggest several promising directions for future analytical and computational investigations.

List of Figures

1.1	Schematic representation of the <i>Volterra's process</i> . A translational	
	mismatch produces a dislocation (a,b,c), while a rotational mismatch	
	produces a disclination (d,e,f). Where b is the Burgers vector, while	ก
1.2	here ϕ is the <i>Frank Angle</i> . Credit: [35, Figure 1]	2
	the red path represents the line defect, and b is the Burgers vector.	
	Credit: [23, Figure 9]	3
1.3	On the left a perfect crystal, where the black arrows represent the circuit Γ ; on the right a crystal with screw dislocation where b is the	
	Burgers vector. Credit: [23, Figure 12]	4
1.4	Formation of a planar wedge disclination: (a) is the negative discli-	
	nation, while (b) is the positive one. Credit: [61, Figure 3]	4
1.5	Scheme of a sample with disclinations. The green point represent a	
	positive disclination, while the orange one a negative disclination. Credit: [32]	5
3.1	A disclination dipole in radial symmetry. The green triangle rep-	
0.1	resents a negative disclination, while the orange one is a positive	
	disclination.	23
3.2	Behavior of the forcing functions of System (3.21)	25
3.3	Zeroes of $f(h,d)$ and $g(h,d)$	26
3.4	Representation of the equilibrium point $E_2 = (1, \frac{1}{2})$. In this scenario	
	the positive disclination (orange triangle) lies on the boundary of	
	the domain, while the negative one (green triangle) is sitting at the	
	center of the disk	28
3.5	Details of the interaction between defects in the presence of numerical	29
3.6	errors using different stiff solvers in Matlab	$\frac{29}{30}$
3.7	Details of the anomaly near $g(h,d) = 0$	31
3.8	Numerical definition of $C \subseteq \Omega_1$ based on different error threshold.	36
J.0	= $=$ $=$ $=$ $=$ $=$ $=$ $=$ $=$ $=$	

3.9	Behavior of the L^{∞} -error as $\kappa \to 0$	40
3.10	Behavior of a dipole of disclinations with a fixed distance, varying	
	h_0 from bottom $h_0 = 0.01$ to top $h_0 = 2 - 2d_0$, with $d_0 = 0.80$ (left)	
	and $d_0 = 0.10$ (right)	48

Bibliography

- [1] R. Alicandro, L. De Luca, A. Garroni, and M. Ponsiglione, «Dynamics of discrete screw dislocations on glide directions», *Journal of the Mechanics and Physics of Solids*, vol. 92, pp. 87–104, 2016.
- [2] R. Alicandro, L. De Luca, M. Palombaro, and M. Ponsiglione, «Γ-convergence analysis of the nonlinear self-energy induced by edge dislocations in semi-discrete and discrete models in two dimensions», *Advances in Calculus of Variations*, vol. 18, no. 1, pp. 1–23, 2025.
- [3] F. Banhart, J. Kotakoski, and A. Krasheninnikov, «Structural defects in graphene», ACS nano, vol. 5, no. 1, pp. 26–41, 2011.
- [4] T. Blass, I. Fonseca, G. Leoni, and M. Morandotti, «Dynamics for systems of screw dislocations», SIAM Journal on Applied Mathematics, vol. 75, no. 2, pp. 393–419, 2015.
- [5] T. Blass and M. Morandotti, «Renormalized energy and Peach-Köhler forces for screw dislocations with antiplane shear», arXiv preprint arXiv:1410.6200, 2014.
- [6] G. A. Bonaschi, P. Van Meurs, and M. Morandotti, «Dynamics of screw dislocations: A generalised minimising-movements scheme approach», *European Journal of Applied Mathematics*, vol. 28, no. 4, pp. 636–655, 2017.
- [7] J. M. Burgers, «Physics.—Some considerations on the fields of stress connected with dislocations in a regular crystal lattice», in *Selected papers of JM Burgers*, Springer, 1939, pp. 335–389.
- [8] P. Cermelli and G. Leoni, «Renormalized energy and forces on dislocations», SIAM journal on mathematical analysis, vol. 37, no. 4, pp. 1131–1160, 2005.
- [9] P. Cermelli and M. E. Gurtin, «The motion of screw dislocations in crystalline materials undergoing antiplane shear: Glide, cross-slip, fine cross-slip», Archive for rational mechanics and analysis, vol. 148, no. 1, pp. 3–52, 1999.

- [10] P. Cesana, L. De Luca, and M. Morandotti, «Semidiscrete modeling of systems of wedge disclinations and edge dislocations via the Airy stress function method», SIAM Journal on Mathematical Analysis, vol. 56, no. 1, pp. 79–136, 2024.
- [11] P. Cesana, A. Grillo, M. Morandotti, and A. Pastore, «Dissipative Dynamics of Volterra Disclinations», SIAM Journal on Applied Mathematics, vol. 85, no. 4, pp. 1361–1386, 2025.
- [12] G. Dal Maso, «Ennio De Giorgi and Γ-convergence», Discrete and Continuous Dynamical Systems, vol. 31, no. 4, pp. 1017–1021, 2011.
- [13] E. De Giorgi, «Sulla convergenza di alcune successioni d'integrali del tipo dell'area», Ennio De Giorgi, vol. 414, p. 64, 1975.
- [14] R. deWit, «Relation between dislocations and disclinations», Journal of Applied Physics, vol. 42, no. 9, pp. 3304–3308, 1971.
- [15] R. deWit, "Theory of disclinations: II. continuous and discrete disclinations in anisotropic elasticity", Journal of Research of the National Bureau of Standards. Section A, Physics and Chemistry, vol. 77, no. 3, p. 359, 1973.
- [16] R. deWit, "Theory of disclinations: III. continuous and discrete disclinations in isotropic elasticity", Journal of Research of the National Bureau of Standards. Section A, Physics and Chemistry, vol. 77, no. 3, p. 359, 1973.
- [17] R. deWit, "Theory of disclinations: IV. Straight disclinations", Journal of Research of the National Bureau of Standards. Section A, Physics and Chemistry, vol. 77, no. 5, p. 607, 1973.
- [18] E. Domoroshchina, A. Dubovskii, G. Kuz'Micheva, and G. Semenkovich, «Influence of point defects on the electrical conductivity and dielectric properties of langasite», *Inorganic materials*, vol. 41, no. 11, pp. 1218–1221, 2005.
- [19] J. Eshelby, «A simple derivation of the elastic field of an edge dislocation», British Journal of Applied Physics, vol. 17, no. 9, p. 1131, 1966.
- [20] F. Frank and W. Read Jr, «Multiplication processes for slow moving dislocations», Physical Review, vol. 79, no. 4, p. 722, 1950.
- [21] A. Garroni, G. Leoni, and M. Ponsiglione, «Gradient theory for plasticity via homogenization of discrete dislocations», *Journal of the European Mathematical Society*, vol. 12, no. 5, pp. 1231–1266, 2010.
- [22] M. Y. Gutkin and E. Aifantis, "Dislocations and disclinations in the gradient theory of elasticity", Physics of the Solid State, vol. 41, no. 12, pp. 1980–1988, 1999.
- [23] A. Haddad, *Difetti dei cristalli*, https://www.gmpe.it/minerali/difetti-cristalli.

- [24] W. Harris, «Disclinations», Scientific American, vol. 237, no. 6, pp. 130–145, 1977.
- [25] J. P. Hirth, G. Hirth, and J. Wang, «Disclinations and disconnections in minerals and metals», *Proceedings of the National Academy of Sciences*, vol. 117, no. 1, pp. 196–204, 2020.
- [26] J. Hirth, «A brief history of dislocation theory», Metallurgical Transactions A, vol. 16, no. 12, pp. 2085–2090, 1985.
- [27] J. Hirth, J. Lothe, and T. Mura, "Theory of dislocations", *Journal of Applied Mechanics*, vol. 50, no. 2, pp. 476–477, 1983.
- [28] P. Holba and D. Sedmidubskỳ, «Crystal defects and nonstoichiometry contributions to heat capacity of solids», in *Thermal analysis of micro, nano-and non-crystalline materials: transformation, crystallization, kinetics and thermodynamics*, Springer, 2012, pp. 53–74.
- [29] T. Hudson and M. Morandotti, «Properties of screw dislocation dynamics: Time estimates on boundary and interior collisions», SIAM Journal on Applied Mathematics, vol. 77, no. 5, pp. 1678–1705, 2017.
- [30] T. Hudson, «An existence result for Discrete Dislocation Dynamics in three dimensions», arXiv preprint arXiv:1806.00304, 2018.
- [31] D. Hull and D. Bacon, Introduction to dislocations. Elsevier, 2011, vol. 37.
- [32] P. Keim, *Topologische Defekte*, https://en.wikipedia.org/wiki/File: Topologische Defekte in 2D.svg.
- [33] Y. Kitano and K. Kifune, «HREM study of disclinations in MgCd ordered alloy», *Ultramicroscopy*, vol. 39, no. 1-4, pp. 279–286, 1991.
- [34] M. Kleman and J. Friedel, "Disclinations, dislocations, and continuous defects: A reappraisal", Reviews of Modern Physics, vol. 80, no. 1, pp. 61–115, 2008.
- [35] S. Kobayashi, K. Takemasa, and R. Tarumi, "Revisiting Volterra defects: Geometrical relation between edge dislocations and wedge disclinations", Royal Society Open Science, vol. 12, no. 7, p. 242213, 2025.
- [36] N. Y. Lin, M. Bierbaum, P. Schall, J. P. Sethna, and I. Cohen, «Measuring nonlinear stresses generated by defects in 3d colloidal crystals», *Nature* materials, vol. 15, no. 11, pp. 1172–1176, 2016.
- [37] A. Love, A treatise on the mathematical theory of elasticity. Courier Corporation, 1927.
- [38] J. Maddocks, «A Model for Disclinations in Nematic Liquid Crystal», 1986.
- [39] G. A. Maugin, Material inhomogeneities in elasticity. CRC Press, 1993.

- [40] A. Mielke and U. Stefanelli, «Linearized plasticity is the evolutionary Γ-limit of finite plasticity», Journal of the European Mathematical Society, vol. 15, no. 3, pp. 923–948, 2013.
- [41] S. Müller, L. Scardia, and C. I. Zeppieri, «Gradient theory for geometrically nonlinear plasticity via the homogenization of dislocations», in *Analysis and computation of microstructure in finite plasticity*, Springer, 2015, pp. 175–204.
- [42] M. Murayama, J. Howe, H. Hidaka, and S. Takaki, «Atomic-level observation of disclination dipoles in mechanically milled, nanocrystalline Fe», *Science*, vol. 295, no. 5564, pp. 2433–2435, 2002.
- [43] F. Nabarro and M. Duesbery, «Dislocations in solids», vol. 11, 2002.
- [44] F. Nabarro and W. Harris, «Presence and function of disclinations in surface coats of unicellular organisms», *Nature*, vol. 232, no. 5310, pp. 423–423, 1971.
- [45] M. Nakai and L. Sario, «Green's function of the clamped punctured disk», The ANZIAM Journal, vol. 20, no. 2, pp. 175–181, 1977.
- [46] A. Needleman, «Discrete defect plasticity and implications for dissipation», European Journal of Mechanics-A/Solids, vol. 100, p. 105 002, 2023.
- [47] D. Omale, P. Ojih, and M. Ogwo, «Mathematical analysis of stiff and non-stiff initial value problems of ordinary differential equation using MATLAB», International journal of scientific & engineering research, vol. 5, no. 9, pp. 49–59, 2014.
- [48] E. Orowan, «Zur kristallplastizität. iii: Über den mechanismus des gleitvorganges», Zeitschrift für Physik, vol. 89, no. 9, pp. 634–659, 1934.
- [49] M. Polanyi, «Über eine Art Gitterstörung, die einen Kristall plastisch machen könnte», Zeitschrift für Physik, vol. 89, no. 9, pp. 660–664, 1934.
- [50] A. Romanov, «Mechanics and physics of disclinations in solids», European Journal of Mechanics-A/Solids, vol. 22, no. 5, pp. 727–741, 2003.
- [51] A. Romanov, M. Rozhkov, and A. Kolesnikova, "Disclinations in polycrystalline graphene and pseudo-graphenes. review", Letters on Materials, vol. 8, no. 4, pp. 384–400, 2018.
- [52] E. V. Safonova, R. A. Konchakov, Y. P. Mitrofanov, N. P. Kobelev, A. Y. Vinogradov, and V. A. Khonik, «Contribution of interstitial defects and anharmonicity to the premelting increase in the heat capacity of single-crystal aluminum», *JETP Letters*, vol. 103, no. 12, pp. 765–768, 2016.
- [53] A. J. C. B. Saint-Venant, Mémoire sur la torsion des prismes. Mallet-Bachelier, 1856, vol. 14.
- [54] H. Seung and D. Nelson, «Defects in flexible membranes with crystalline order», *Physical Review A*, vol. 38, no. 2, p. 1005, 1988.

- [55] V. Taupin, L. Capolungo, C. Fressengeas, M. Upadhyay, and B. Beausir, «A mesoscopic theory of dislocation and disclination fields for grain boundary-mediated crystal plasticity», *International Journal of Solids and Structures*, vol. 71, pp. 277–290, 2015.
- [56] G. Taylor, «The mechanism of plastic deformation of crystals», Proceedings of the Royal Society of London. Series A, Containing Papers of a Mathematical and Physical Character, vol. 145, no. 855, pp. 362–387, 1934.
- [57] V. Vitek and M. Kléman, «Surface disclinations in nematic liquid crystals», Journal de Physique, vol. 36, no. 1, pp. 59–67, 1975.
- [58] V. Volterra, «Sur l'équilibre des corps élastiques multiplement connexes», in Annales scientifiques de l'École normale supérieure, vol. 24, 1907, pp. 401–517.
- [59] W. Wan, C. Tang, A. Qiu, and Y. Xiang, "The size effects of point defect on the mechanical properties of monocrystalline silicon: A molecular dynamics study", *Materials*, vol. 14, no. 11, p. 3011, 2021.
- [60] M. J. Whelan, P. B. Hirsch, R. Horne, and W. Bollmann, "Dislocations and stacking faults in stainless steel", Proceedings of the Royal Society of London. Series A. Mathematical and Physical Sciences, vol. 240, no. 1223, pp. 524–538, 1956.
- [61] C. Zhang and A. Acharya, «On the relevance of generalized disclinations in defect mechanics», *Journal of the Mechanics and Physics of Solids*, vol. 119, pp. 188–223, 2018.
- [62] J. Zimmer, «Disclinations in a lamellar liquid crystal.», Ph.D. dissertation, Purdue University, 1978.